INTERNATIONAL JOURNAL OF
NUMERICAL ANALYSIS AND MODELING
Volume 21, Number 4, Pages 504–527

doi: 10.4208/ijnam2024-1020

MIXED VIRTUAL ELEMENT METHOD FOR LINEAR PARABOLIC INTEGRO-DIFFERENTIAL EQUATIONS

MEGHANA SUTHAR AND SANGITA YADAV

Abstract. This article develops and analyses a mixed virtual element scheme for the spatial discretization of linear parabolic integro-differential equations (PIDEs) combined with backward Euler's temporal discretization approach. The introduction of mixed Ritz-Volterra projection significantly helps in managing the integral terms, yielding optimal convergence of order $O(h^{k+1})$ for the two unknowns $p(\boldsymbol{x},t)$ and $\boldsymbol{\sigma}(\boldsymbol{x},t)$. In addition, a step-by-step analysis is proposed for the super convergence of the discrete solution of order $O(h^{k+2})$. The fully discrete case has also been analyzed and discussed to achieve $O(\tau)$ in time. Several computational experiments are discussed to validate the proposed schemes computational efficiency and support the theoretical conclusions.

Key words. Mixed virtual element method, parabolic integro-differential equation, error estimates, super-convergence.

1. Introduction

Mathematical models for solving the electrical circuit problems specified by the Kirchhoff voltage laws [34], for a disease transmitted through the movement of contagious individuals [29], heat flow in a substance with memory [30], etc., give rise to the linear integro-differential equations. With consideration for the diverse array of applications of these equations across various domains, our focus lies in the exploration of PIDEs of the following form:

(1)

$$p_t(\boldsymbol{x},t) - \nabla\cdot\left(a(x)\nabla p(\boldsymbol{x},t) - \int_0^t b(x;t,s)\nabla p(\boldsymbol{x},s)ds\right) = f(\boldsymbol{x},t)\ (\boldsymbol{x},t)\in\mathcal{D}\times(0,T],$$
$$p(\boldsymbol{x},t) = 0 \quad (\boldsymbol{x},t)\in\partial\mathcal{D}\times(0,T],$$
$$p(\boldsymbol{x},0) = p_0(\boldsymbol{x}) \quad \boldsymbol{x}\in\mathcal{D}.$$

Here, $\mathcal{D}\subset\mathbb{R}^2$ is a bounded polygon domain having $\partial\mathcal{D}$ as the boundary; furthermore, the interval $[0,T]$ represents a finite time span. This article intends to introduce and examine the mixed virtual element method (VEM) concerning PIDEs (1), with the primary goal of studying the effect of time discretization on virtual element solution. For our analysis, we would require the assumptions listed below on the coefficients and the function f:

H.1 the coefficient $a(x)$ is bounded, positive i.e. $a(x)\geq\mu_0>0$, and smooth enough,

H.2 the coefficient $b(x;t,s)$ and its derivative $b_t(x;t,s)$, $b_s(x;t,s)$ are real-valued, bounded, and smooth,

H.3 the function f is real-valued and smooth enough.

In literature, various approaches have been made to obtain the numerical solution to these equations and related problems, such as the finite element method (FEM) [23, 14], finite volume method [16], VEM [40], least-square Galerkin method [24], *hp*-local discontinuous Galerkin method [32], spectral method [19], HDG method

Received by the editors on September 22, 2023 and, accepted on April 21, 2024.
2000 *Mathematics Subject Classification.* 65M15, 65N12, 65N15.

[26] etc. Further, by extending these ideas in [31, 12, 20], fully discrete schemes were proposed in which discretization of time is implemented using implicit finite difference schemes. The reason for employing finite element scheme and their variants is the computational efficiency and well-established theory of these methods. We stress that polygonal meshes have many benefits: greater flexibility in the meshing of arbitrary geometries, better accuracy in the numerical solution over that obtainable using triangular and quadrilateral meshes on a given nodal grid, and many more, see [36]. To deal with polygonal meshes, VEM was introduced in [1] and is very much appreciated by the scientific community. A detailed study shows that this method can be considered as a generalization of the standard FEM over general polygonal and polyhedral meshes as the convergence analysis of this method can be placed within the structure of the FEM, which is well developed in the literature. In general, VEM has been successfully applied for an approximate estimation of various partial differential equations; for recent developments and applications of this method, we refer to [38, 39, 6, 2, 38] and references within.

One of our concerns in (1) is determining the flux or velocity in addition to the pressure; the typical Galerkin method yields a loss of precision because it is estimated from the approximated solution via post-processing. The mixed methods, on the other hand, provide a direct estimate of this physical quantity and lead to locally conservative solutions. Another advantage of using a mixed technique here is the ability to introduce one more unknown of physical importance, which may be computed directly without adding any new sources of error. Mixed VEM has been effectively employed to approximate a number of partial differential equations; see [9, 8, 10, 21, 11, 22] and references therein for details. Here, we introduce $\boldsymbol{\sigma}(\boldsymbol{x}, t)$, defined by

$$\boldsymbol{\sigma}(\boldsymbol{x}, t) = a(x)\nabla p(\boldsymbol{x}, t) - \int_0^t b(x; t, s)\nabla p(\boldsymbol{x}, s)ds, \tag{2}$$

and rewrite (1) as:

$$p_t(\boldsymbol{x}, t) - \nabla \cdot \boldsymbol{\sigma}(\boldsymbol{x}, t) = f(\boldsymbol{x}, t). \tag{3}$$

The meaning of this independent variable '$\boldsymbol{\sigma}$' is velocity field while discussing flow in porous media, whereas (3) expresses a mass balance in any subdomain of $\mathcal{D}$, see[35]. So, the mixed formulation for this setting simultaneously approximates the pressure and the velocity field while maintaining the underlying local mass conservation. Since there is an integral term in (2) which involves ∇p, we introduce a new kernel known as the resolvent kernel to deal with this integral term. This formulation has been explored in [35, 17, 18] for the semi-discrete formulation and non-smooth initial data, but the fully-discrete case has not been explored yet for this formulation to the best of our knowledge.

For the mixed variational formulation corresponding to (2), we will use the resolvent kernel, applicable to any Volterra integral equation of the second kind [33], which takes the form:

$$X(t) = F(t) + \int_0^t K(t, s)X(s)ds. \tag{4}$$

The resolvent kernel for (4) can be expressed as:

$$X(t) = F(t) + \int_0^t R(t, s)F(s)ds.$$

Moreover, the resolvent kernel of (4) satisfies:

$$R(t,s) = K(t,s) + \int_t^s K(t,z)R(z,s)dz.$$

Although determining the resolvent kernel for a given kernel may be a challenging task, but computationally, this approach proves significantly more efficient. This is particularly evident when comparing it to the formulation outlined in [27], which involves two terms under the integral sign and hence requires $N \times N$ times more computation of a matrix. Additionally, in the 3-field formulation discussed in [28], the system of equations is considerably larger than the system arising from this formulation. Hence, whenever the resolvent kernel is available, utilizing this formulation yields computational cost cutting. Furthermore, if the resolvent kernel turns out to be a series, we can truncate the series and get the desired result as shown by Example 3 in Section 5.

There is hardly any result in mixed VEM applied to PIDEs, so an effort has been made to address this shortcoming. With the computational benefits and polygonal meshes in mind, we plan to employ mixed VEM for a certain class of PIDEs to conduct an in-depth analysis of the convergence behavior of PIDEs.

This paper implements the mixed VEM method on (1). This work presents several significant contributions, which are outlined as follows:

- To tackle the integral term, an approach involving a novel projection with a memory term (referred to as mixed Ritz-Volterra (R.V.) projection) is introduced, which helps in achieving the optimal convergence of order $O(h^{k+1})$ for both the unknowns.
- A fully discretized scheme is put forth, utilizing the backward Euler's method for temporal derivative and the left rectangular rule for the discretization of the integral term.
- The analysis is performed to show the super convergence of the discrete solution, which has been verified with the different numerical experiments.
- Theoretical results have been validated through the implementation of numerical experiments.

Unlike finite element formulation, virtual element discretization necessitates using the L^2 projection operator, complicating the convergence analysis.

Throughout the article, for a bounded polygon domain $\mathcal{D}$ and an integer $m \geq 0$, we employ conventional notation $(\cdot,\cdot)_{m,\mathcal{D}}$ and $\|\cdot\|_{m,\mathcal{D}}$ to denote the $H^m(\mathcal{D})$ inner product and norm. Furthermore, we write commonly $(\cdot,\cdot)$ and $\|\cdot\|$ to indicate the L^2 inner product and norm. Also, $|\cdot|_{m,\mathcal{D}}$ symbolises the $H^m(\mathcal{D})$ semi-norm. The space X_q^m, for $q = 1, 2$ with the standard modification for $q = \infty$ is defined as:

$$X_q^m = \{v(\boldsymbol{x},t) \in H^m(\mathcal{D}) \text{ for a.e. } t \in (0,T] \text{ and } \left(\int_0^T \|v(\cdot,t)\|_m^q dt\right)^{1/q} < \infty\},$$

with the norm

$$\|v\|_{X_q^m} = \left(\int_0^T \|v(\cdot,t)\|_m^q dt\right)^{1/q} \qquad \|v\|_{X_\infty^m} = \sup_{0\leq t\leq T} \|v(\cdot,t)\|_m.$$

We consider the space $\mathcal{V} = H(\text{div};\mathcal{D})$ and $\mathcal{Q} = L^2(\mathcal{D})$, whereas the spaces $H(\text{div};\mathcal{D})$ and $H(\text{rot};\mathcal{D})$ is defined as:

$$H(\text{div};\mathcal{D}) = \{\boldsymbol{\chi} \in (\mathcal{Q})^2 : \text{div } \boldsymbol{\chi} \in \mathcal{Q}\},$$
$$H(\text{rot};\mathcal{D}) = \{\boldsymbol{\chi} \in (\mathcal{Q})^2 : rot\, \boldsymbol{\chi} \in \mathcal{Q}\}.$$

For more details about these spaces, see [3]. The upcoming sections are organized as follows: Section 2 presents the introduction of virtual element spaces along with the variational and semi-discrete VEM formulation. The analysis of convergence for the semi-discrete scheme is conducted in Section 3 by introducing a mixed R.V. projection depending on the memory term. Also, the super convergence property is discussed in the same section. Section 4 outlines the fully discrete scheme and its convergence analysis. Lastly, Section 5 contains details of distinct numerical experiments aimed at validating the theoretical findings presented in Sections 3, and 4.

2. VEM Approximation

2.1. Virtual Element Space. We assume $\mathcal{I}_h$ to be the collection of decomposition of $\mathcal{D}$ into star-shaped sub-polygons E, and $\mathcal{E}_h$ is the set of edges e of $\mathcal{I}_h$. Along with this, we postulate that for each element E, $\exists$ a $\delta_E > 0$ such that E is star-shaped from every point of the disc D_{δ_E} with radius $\delta_E h_E$ (h_E represents the element E's diameter), while h_e represents the edge e's length, of the element E and fulfills $h_e \geq \delta_E h_E$. While considering a sequence of decomposition $\{\mathcal{I}_h\}_h$, we assume $\delta_E \geq \delta_0 > 0$ for some δ_0 independent of E and $\mathcal{I}_h$. The largest diameter of $\mathcal{I}_h$'s elements is h, as is customary. Here, $\mathbb{P}_k(E)$ is the set consisting of polynomials of degree $\leq k$ in E. Moreover, the mesh assumptions can be significantly relaxed with some changes in the interpolation estimates, stability term, etc., as discussed in Remark 3.3 of [4] and further elaborated in [13, 25, 7]. Now, we define the local space

$$V_h^k(E) = \{\boldsymbol{\chi} \in H(\mathrm{div}; E) \cap H(\mathrm{rot}; E) : \boldsymbol{\chi} \cdot \boldsymbol{n}_{|e} \in \mathbb{P}_k(e)\ \forall e \in \partial E, \quad \nabla \cdot \boldsymbol{\chi} \in \mathbb{P}_k(E) \\ \text{and, rot } \boldsymbol{\chi} \in \mathbb{P}_{k-1}(E), \text{ for } k \geq 0\},$$

where $\mathbb{P}_{-1}(E) = \{0\}$. For our analysis, we define the discrete spaces as:

$$V_h^k := \{\boldsymbol{\chi} \in \mathcal{V} :\ \boldsymbol{\chi}_{|E} \in V_h^k(E) \quad \forall\, E \text{ in } \mathcal{I}_h\},$$
$$Q_h^k := \{q \in L^2(\mathcal{D}) :\ q_{|E} \in \mathbb{P}_k(E) \quad \forall\, E \text{ in } \mathcal{I}_h\}.$$

The discrete bilinear forms in spaces V_h^k and Q_h^k can be computed via degrees of freedom (dof). For the space Q_h^k, we are considering the scaled monomials on each element E as dof:

$$\left(1, \left(\frac{x - x_{c_E}}{h_E}\right), \left(\frac{y - y_{c_E}}{h_E}\right)\right) \quad \text{for } k = 1;$$

$$\left(1, \left(\frac{x - x_{c_E}}{h_E}\right), \left(\frac{y - y_{c_E}}{h_E}\right), \left(\frac{x - x_{c_E}}{h_E}\right)^2, \left(\frac{x - x_{c_E}}{h_E}\right)\left(\frac{y - y_{c_E}}{h_E}\right), \left(\frac{y - y_{c_E}}{h_E}\right)^2\right)$$

for $k = 2$, and in a similar way for a higher value of k, where (x_{c_E}, y_{c_E}) and h_E represents the centroid and diameter of the polygon E, respectively. For the local space $V_h^k(E)$, we present the well-defined collection of operators as dof, see [4]:

- $\displaystyle\int_e \boldsymbol{\chi} \cdot \boldsymbol{n} q_k d\gamma$ for each edge e of the element E, $\forall q_k \in \mathbb{P}_k(e)$,
- $\displaystyle\int_E \boldsymbol{\chi} \cdot \boldsymbol{g}_{k-1} d\boldsymbol{x}, \quad \forall \boldsymbol{g}_{k-1} \in \nabla \mathbb{P}_k(E)$,
- $\displaystyle\int_E \boldsymbol{\chi} \cdot \boldsymbol{g}_k^{\perp} d\boldsymbol{x}, \quad \forall \boldsymbol{g}_k^{\perp} \in L^2(E)$ orthogonal of $\nabla \mathbb{P}_{k+1}(E)$ in $(\mathbb{P}_k(E))^2$.

To define discrete variational formulation, we make use of the L^2-projection operators denoted by $\Pi_k^0 : \mathcal{Q} \to Q_h^k$ and $\mathbf{\Pi}_k^0 : \mathcal{V} \to V_h^k$, and defined for any $q \in \mathcal{Q}$ and $\boldsymbol{\chi} \in \mathcal{V}$ as:

$$\int_E (q - \Pi_k^0 q) p_k d\boldsymbol{x} = 0 \quad \forall p_k \in \mathbb{P}_k(E), \quad \forall E \in \mathcal{I}_h,$$
$$\int_E (\boldsymbol{\chi} - \mathbf{\Pi}_k^{\mathbf{0}} \boldsymbol{\chi}) \boldsymbol{p_k} d\boldsymbol{x} = 0 \quad \forall \boldsymbol{p_k} \in (\mathbb{P}_k(E))^2, \quad \forall E \in \mathcal{I}_h.$$

Π_k^0 and $\mathbf{\Pi}_k^{\mathbf{0}}$ satisfies the following estimates, see[4]:

$$||q - \Pi_k^0 q||_0 \leq Ch^r |q|_r, \qquad ||\boldsymbol{\chi} - \mathbf{\Pi}_k^{\mathbf{0}} \boldsymbol{\chi}||_0 \leq Ch^r |\boldsymbol{\chi}|_r \quad 0 \leq r \leq k+1. \tag{5}$$

Now, define "Fortin" operator $\mathbf{\Pi}_h^F$: $(H^1(\mathcal{D}))^2 \to V_h^k$ through the dof of the space V_h^k as:

- $\int_e (\boldsymbol{\chi} - \mathbf{\Pi}_h^F \boldsymbol{\chi}) \cdot \boldsymbol{n} q_k d\gamma = 0$ for each edge e, $\forall q_k \in \mathbb{P}_k(E)$,
- $\int_E (\boldsymbol{\chi} - \mathbf{\Pi}_h^F \boldsymbol{\chi}) \cdot \boldsymbol{g}_{k-1} d\boldsymbol{x} = 0$ for each element E, $\forall \boldsymbol{g}_{k-1} \in \nabla \mathbb{P}_k(E)$,
- $\int_E (\boldsymbol{\chi} - \mathbf{\Pi}_h^F \boldsymbol{\chi}) \cdot \boldsymbol{g}_k^{\perp} d\boldsymbol{x} = 0$ for each element E, $\forall \boldsymbol{g}_k^{\perp} \in L^2(E)$ orthogonal of $\nabla \mathbb{P}_{k+1}(E)$ in $(\mathbb{P}_k(E))^2$.

$\mathbf{\Pi}_h^F$ satisfy the following properties and estimates:

$$\nabla \cdot \mathbf{\Pi}_h^F \boldsymbol{\chi} = \Pi_k^0 \nabla \cdot \boldsymbol{\chi},$$

$$||\boldsymbol{\chi} - \mathbf{\Pi}_h^F \boldsymbol{\chi}||_0 \leq Ch^r |\boldsymbol{\chi}|_r, \quad \|\nabla \cdot (\boldsymbol{\chi} - \mathbf{\Pi}_h^F \boldsymbol{\chi})\|_0 \leq Ch^r |\nabla \cdot \boldsymbol{\chi}|_r \quad 0 \leq r \leq k+1. \tag{6}$$

For more details about $\mathbf{\Pi}_h^F$, we refer to [37].

2.2. The Continuous and Semi-discrete Formulation. Assuming $\mu(x) = a^{-1}(x)$, (2) becomes:

$$\nabla p(\boldsymbol{x}, t) = \mu(x) \boldsymbol{\sigma}(\boldsymbol{x}, t) + \int_0^t \mu(x) b(x; t, s) \nabla p(\boldsymbol{x}, s) ds,$$

which can be rewritten as:

$$\nabla p(\boldsymbol{x}, t) = \mu(x) \boldsymbol{\sigma}(\boldsymbol{x}, t) + \int_0^t \mathcal{R}(x; t, s) \mu(x) \boldsymbol{\sigma}(\boldsymbol{x}, s) ds.$$

where $\mathcal{R}(x; t, s)$ is the resolvent kernel of $\mu(x) b(x; t, s)$, see [33, 35, 17] and satisfy the following:

$$\mathcal{R}(x; t, s) = \mu(x) b(x; t, s) + \int_s^t \mu(x) b(x; t, z) \mathcal{R}(x; z, s) dz \quad t > s \geq 0.$$

One of the possible ways of finding a resolvent kernel $R(t, s)$ for any kernel $K(t, s)$ is:

$$R(t, s) = \sum_{m=1}^{\infty} K_m(t, s),$$

where $K_m(t, s)$ is given by:

$$K_1(t, s) = K(t, s); \quad K_m(t, s) = \int_s^t K(t, z) K_{m-1}(z, s) dz. \tag{7}$$

The smoothness and boundedness of the resolvent kernel are derived from the smoothness and boundedness of $a^{-1}(x) b(x; t, s)$. For further details, please see [17].

By denoting $\mathcal{K}(x;t,s) = \mathcal{R}(x;t,s)\mu(x)$, we define variational formulation as: Find $(p,\boldsymbol{\sigma}) \in L^2(0,T;\mathcal{Q}) \times L^2(0,T;\mathcal{V})$, for a.e. t in $(0,T)$, see [15] such that:

$$\begin{aligned} (p_t,\phi) - (\nabla\cdot\boldsymbol{\sigma},\phi) &= (f,\phi) \ \ \forall \phi \in \mathcal{Q}, \\ (\mu\boldsymbol{\sigma},\boldsymbol{\chi}) + \int_0^t (\mathcal{K}(t,s)\boldsymbol{\sigma}(s),\boldsymbol{\chi})ds + (\nabla\cdot\boldsymbol{\chi},p) &= 0 \ \ \forall \boldsymbol{\chi} \in \mathcal{V}. \end{aligned} \tag{8}$$

with the initial condition $p(\cdot,0) = p_0$.

Now, the mixed VEM formulation reads as: Find $(p_h,\boldsymbol{\sigma}_h) \in L^2(0,T;\mathcal{Q}_h^k) \times L^2(0,T;\mathcal{V}_h^k)$, for a.e. t in $(0,T)$ such that:

$$\begin{aligned} (p_{h,t},\phi_h) - (\nabla\cdot\boldsymbol{\sigma}_h,\phi_h) &= (f,\phi_h) \quad \forall \phi_h \in Q_h^k, \\ a_h(\boldsymbol{\sigma}_h,\boldsymbol{\chi}_h) + \int_0^t \mathcal{K}_h(t,s;\boldsymbol{\sigma}_h(s),\boldsymbol{\chi}_h)ds + (\nabla\cdot\boldsymbol{\chi}_h,p_h) &= 0 \quad \forall \boldsymbol{\chi}_h \in V_h^k, \end{aligned} \tag{9}$$

where the initial condition $p_h(\cdot,0)$ follows Remark 2 and [40]. The discrete bilinear forms above are defined $\forall \boldsymbol{z}_h,\boldsymbol{\chi}_h \in V_h^k$ as:

$$a_h(\boldsymbol{z}_h,\boldsymbol{\chi}_h) := \sum_{E\in\mathcal{I}_h} a_h^E(\boldsymbol{z}_h,\boldsymbol{\chi}_h), \qquad \mathcal{K}_h(t,s;\boldsymbol{z}_h,\boldsymbol{\chi}_h) := \sum_{E\in\mathcal{I}_h} \mathcal{K}_h^E(t,s;\boldsymbol{z}_h,\boldsymbol{\chi}_h),$$

and bilinear forms $a_h^E(\cdot,\cdot) : V_h^k(E)\times V_h^k(E) \to \mathbb{R}$ and $\mathcal{K}_h^E(\cdot,\cdot) : V_h^k(E)\times V_h^k(E) \to \mathbb{R}$, on every element $E \in \mathcal{I}_h$ are defined as:

$$\begin{aligned} a_h^E(\boldsymbol{l}_h,\boldsymbol{q}_h) &:= (\mu\boldsymbol{\Pi}_k^0\boldsymbol{l}_h,\boldsymbol{\Pi}_k^0\boldsymbol{q}_h)_{0,E} + S_0^E((I-\boldsymbol{\Pi}_k^0)\boldsymbol{l}_h,(I-\boldsymbol{\Pi}_k^0)\boldsymbol{q}_h) \quad \forall \boldsymbol{l}_h,\boldsymbol{q}_h \in V_h^k(E), \\ \mathcal{K}_h^E(t,s;\boldsymbol{l}_h,\boldsymbol{q}_h) &:= (\mathcal{K}(t,s)\boldsymbol{\Pi}_k^0\boldsymbol{l}_h,\boldsymbol{\Pi}_k^0\boldsymbol{q}_h)_{0,E} \quad \forall \boldsymbol{l}_h,\boldsymbol{q}_h \in V_h^k(E). \end{aligned}$$

The stability term $S_0^E : V_h^k(E)\times V_h^k(E) \to \mathbb{R}$ should be constructed in such a way that, $\exists\, \mu_*,\mu^*$ independent of h with $0 < \mu_* \le \mu^*$ and satisfies the following:

$$\mu_* a^E(\boldsymbol{l}_h,\boldsymbol{l}_h) \le S_0^E(\boldsymbol{l}_h,\boldsymbol{l}_h) \le \mu^* a^E(\boldsymbol{l}_h,\boldsymbol{l}_h) \quad \forall \boldsymbol{l}_h \in V_h^k(E).$$

One of the possible choices of $S_0^E(\cdot,\cdot)$ is:

$$S_0^K((I-\Pi_k^0)\boldsymbol{l}_h,(I-\Pi_k^0)\boldsymbol{m}_h) := \bar{\mu}|E| \sum_{i=1}^{N_{\mathrm{dof}}} \mathrm{dof}_i(\boldsymbol{l}_h - \boldsymbol{\Pi}_k^0\boldsymbol{l}_h)\mathrm{dof}_i(\boldsymbol{m}_h - \boldsymbol{\Pi}_k^0\boldsymbol{m}_h),$$

where $\bar{\mu}$ is some positive constant approximation of the coefficients $\mu(x)$ [5]. Moreover, $\exists\, \mu_1,\mu_2 > 0$, such that:

$$a_h(\boldsymbol{\chi}_h,\boldsymbol{\chi}_h) \ge \mu_1\|\boldsymbol{\chi}_h\|^2 \text{ and } |a_h(\boldsymbol{z}_h,\boldsymbol{\chi}_h)| \le \mu_2\|\boldsymbol{z}_h\|\|\boldsymbol{\chi}_h\| \quad \forall \boldsymbol{\chi}_h \in V_h^k. \tag{10}$$

For more details about S_0^E and its properties, see [5, 4].

Remark 1. *Adding the stability term S_0^E in $a_h^E(\cdot,\cdot)$ helps to prove the coercivity of a_h^E. However, since we only need $\mathcal{K}_h^E(\cdot,\cdot)$ to be bounded, therefore we don't need to add this extra term $\mathcal{K}_h^E(\cdot,\cdot)$, see* [40].

3. Error Analysis for the Semi-discrete Case

Lemma 1. *For $E \in \mathcal{I}_h$, let the coefficients $\mu(x)$ and $\mathcal{K}(x;t,s)$ be smooth scaler-valued functions in $\mathcal{D}$ and $\boldsymbol{u}$ be smooth vector-valued function and $\boldsymbol{\chi}_h \in V_h^k(E)$. Then,*

$$\begin{aligned} a_h^E(\boldsymbol{\Pi}_k^0\boldsymbol{u},\boldsymbol{\chi}_h) - (\mu\boldsymbol{\Pi}_k^0\boldsymbol{u},\boldsymbol{\chi}_h)_{0,E} &\le C_\mu h^{k+1}|\boldsymbol{u}|_{k+1,E}|\boldsymbol{\chi}_h|_{0,E}, \\ \mathcal{K}_h(t,s;\boldsymbol{\Pi}_k^0\boldsymbol{u},\boldsymbol{\chi}_h) - (\mathcal{K}(t,s)\boldsymbol{\Pi}_k^0\boldsymbol{u},\boldsymbol{\chi}_h)_{0,E} &\le C_{\mathcal{K}} h^{k+1}|\boldsymbol{u}|_{k+1,E}|\boldsymbol{\chi}_h|_{0,E}. \end{aligned} \tag{11}$$

Proof. Let $\boldsymbol{l}_h, \boldsymbol{\chi}_h$ be vector-valued functions in $V_h^k(E)$. Then, by using the properties of $\boldsymbol{\Pi}_k^0$, we arrive at:

$$
\begin{aligned}
&a_h^E(\boldsymbol{l}_h, \boldsymbol{\chi}_h) - (\mu \boldsymbol{l}_h, \boldsymbol{\chi}_h)_{0,E} \\
&= (\mu \boldsymbol{l}_h - \boldsymbol{\Pi}_k^0(\mu \boldsymbol{l}_h), \boldsymbol{\chi}_h - \boldsymbol{\Pi}_k^0 \boldsymbol{\chi}_h)_{0,E} + (\boldsymbol{l}_h - \boldsymbol{\Pi}_k^0 \boldsymbol{l}_h, \mu \boldsymbol{\chi}_h - \boldsymbol{\Pi}_k^0(\mu \boldsymbol{\chi}_h))_{0,E} \\
&\quad - (\boldsymbol{l}_h - \boldsymbol{\Pi}_k^0 \boldsymbol{l}_h, \mu(\boldsymbol{\chi}_h - \boldsymbol{\Pi}_k^0 \boldsymbol{\chi}_h))_{0,E} + S_0^E((I - \boldsymbol{\Pi}_k^0)\boldsymbol{l}_h, (I - \boldsymbol{\Pi}_k^0)\boldsymbol{\chi}_h).
\end{aligned} \tag{12}
$$

Now, put $\boldsymbol{l}_h = \boldsymbol{\Pi}_k^0 \boldsymbol{u}$ in (12) and using the properties of $\boldsymbol{\Pi}_k^0$, last three terms becomes zero and we arrive at:

$$
a_h^E(\boldsymbol{\Pi}_k^0 \boldsymbol{u}, \boldsymbol{\chi}_h) - (\mu \boldsymbol{\Pi}_k^0 \boldsymbol{u}, \boldsymbol{\chi}_h)_{0,E} \leq C_\mu h^{k+1} |\boldsymbol{u}|_{k+1,E} |\boldsymbol{\chi}_h|_{0,E}.
$$

Using the similar arguments, we can also prove (11). □

3.1. Mixed Ritz Volterra Projection. For the formulation described in (8) and (9), we can now derive the optimal error estimates for both the semi-discrete and fully-discrete cases, we need to deal with the memory term. Therefore, we introduce a new projection here with the memory term known as mixed R.V.projection. Given $(p(t), \boldsymbol{\sigma}(t)) \in Q \times V$ for $t \in (0, T]$, define mixed R.V. projection $(\tilde{p}(t), \tilde{\boldsymbol{\sigma}}(t)) \in Q_h^k \times V_h^k$, as:

$$
\begin{aligned}
&a_h(\tilde{\boldsymbol{\sigma}}, \boldsymbol{\chi}_h) + \int_0^t \mathcal{K}_h(t, s; \tilde{\boldsymbol{\sigma}}(s), \boldsymbol{\chi}_h) ds + (\nabla \cdot \boldsymbol{\chi}_h, \tilde{p}) \\
&\qquad = (\mu \boldsymbol{\sigma}, \boldsymbol{\chi}_h) + \int_0^t (\mathcal{K}(t, s) \boldsymbol{\sigma}(s), \boldsymbol{\chi}_h) ds + (\nabla \cdot \boldsymbol{\chi}_h, p) \quad \forall \boldsymbol{\chi}_h \in V_h^k, \\
&(\nabla \cdot (\boldsymbol{\sigma} - \tilde{\boldsymbol{\sigma}}), \phi_h) = 0 \quad \forall \phi_h \in Q_h^k.
\end{aligned} \tag{13}
$$

Since (13) is a linear system. To prove the existence and uniqueness of the mixed R.V. projection, it is sufficient to prove that the associated homogenous system (14)-(15) has only a trivial solution.

$$
a_h(\tilde{\boldsymbol{\sigma}}, \boldsymbol{\chi}_h) + \int_0^t \mathcal{K}_h(t, s; \tilde{\boldsymbol{\sigma}}(s), \boldsymbol{\chi}_h) ds + (\nabla \cdot \boldsymbol{\chi}_h, \tilde{p}) = 0 \quad \forall \boldsymbol{\chi}_h \in V_h^k, \tag{14}
$$

$$
(\nabla \cdot \tilde{\boldsymbol{\sigma}}, \phi_h) = 0 \quad \forall \phi_h \in Q_h^k. \tag{15}
$$

Put $\phi_h = \nabla \cdot \tilde{\boldsymbol{\sigma}}$ in (15) to arrive at $\nabla \cdot \tilde{\boldsymbol{\sigma}} = 0$. Substitute $\boldsymbol{\chi}_h = \tilde{\boldsymbol{\sigma}}$ in (14) and by using (10), we arrive at the following:

$$
\mu_1 \|\tilde{\boldsymbol{\sigma}}\|^2 \leq - \int_0^t \mathcal{K}_h(t, s; \tilde{\boldsymbol{\sigma}}(s), \tilde{\boldsymbol{\sigma}}) ds
$$

$$
\|\tilde{\boldsymbol{\sigma}}\| \leq C \int_0^t \|\tilde{\boldsymbol{\sigma}}(s)\| ds
$$

Using Grönwall's lemma, we have $\|\tilde{\boldsymbol{\sigma}}\| = 0$ Now, we use the *inf-sup* condition mentioned in [4], [8], which is:

$$
\exists\ \beta > 0 \text{ such that } \inf_{q \in Q_h^k} \sup_{v \in V_h^k} \frac{(\nabla \cdot \boldsymbol{v}, q)}{\|q\|_Q \|\boldsymbol{v}\|_V} \geq \beta > 0.
$$

So,

$$
\|\tilde{p}\| \leq c \sup_{v \in V_h^k} \frac{(\nabla \cdot \boldsymbol{\chi}_h, \tilde{p})}{\|\boldsymbol{\chi}_h\|_V} \leq C \left(\|\tilde{\boldsymbol{\sigma}}\| + \int_0^t \|\tilde{\boldsymbol{\sigma}}(s)\| ds \right).
$$

We arrive at $\|\tilde{p}\| = 0$. Hence, $\tilde{p} = 0$ and $\tilde{\boldsymbol{\sigma}} = 0$.

Below, we present the estimates for R.V. projection:

Theorem 1. *Under the assumptions* H.1-H.3, $\boldsymbol{\sigma}$ *and* $p \in X_\infty^{k+1}$, $\exists$ *a unique solution* $(\tilde{p}, \tilde{\boldsymbol{\sigma}}) \in Q_h^k \times V_h^k$, *which satisfies* (13). *Furthermore, the following estimates hold true:*

$$\|\boldsymbol{\sigma} - \tilde{\boldsymbol{\sigma}}\|_{X_\infty^0} \leq Ch^{k+1} \left(|\boldsymbol{\sigma}|_{k+1} + \int_0^t |\boldsymbol{\sigma}(s)|_{k+1} ds \right), \tag{16}$$

$$\|p - \tilde{p}\|_{X_\infty^0} \leq Ch^{k+1} \left(|p|_{k+1} + |\boldsymbol{\sigma}|_{k+1} + \int_0^t |\boldsymbol{\sigma}(s)|_{k+1} ds \right). \tag{17}$$

Proof. In order to prove (16) and (17), we proceed by considering $\boldsymbol{\vartheta} = \boldsymbol{\sigma} - \tilde{\boldsymbol{\sigma}}$, $\boldsymbol{\psi}_h = \boldsymbol{\Pi}_{\boldsymbol{h}}^{\boldsymbol{F}} \boldsymbol{\sigma} - \tilde{\boldsymbol{\sigma}}$, $\rho = p - \tilde{p}$, and $\tau_h = \Pi_k^0 p - \tilde{p} \in Q_h^k$. Now, By the definition of the mixed R.V. projection (13):

(18)

$$\begin{aligned} a_h(\boldsymbol{\Psi}_{\boldsymbol{h}}, \boldsymbol{\chi}_h) + \int_0^t \mathcal{K}_h(t,s; \boldsymbol{\Psi}_{\boldsymbol{h}}(s), \boldsymbol{\chi}_h) ds \\ = (\nabla \cdot \boldsymbol{\chi}_h, \tilde{p} - p) + \left(\int_0^t \mathcal{K}_h(t,s; \boldsymbol{\Pi}_{\boldsymbol{h}}^{\boldsymbol{F}} \boldsymbol{\sigma}(s), \boldsymbol{\chi}_h) ds - \int_0^t (\mathcal{K}(t,s) \boldsymbol{\sigma}(s), \boldsymbol{\chi}_h) ds \right) \\ + \left(a_h(\boldsymbol{\Pi}_{\boldsymbol{h}}^{\boldsymbol{F}} \boldsymbol{\sigma}, \boldsymbol{\chi}_h) - (\mu \boldsymbol{\sigma}, \boldsymbol{\chi}_h) \right). \end{aligned}$$

For solving the third term in the right-hand side of (18), we use Lemma 1, (10) and Cauchy-Schwarz inequality as:

(19)

$$\begin{aligned} & a_h(\boldsymbol{\Pi}_{\boldsymbol{h}}^{\boldsymbol{F}} \boldsymbol{\sigma}, \boldsymbol{\chi}_h) - (\mu \boldsymbol{\sigma}, \boldsymbol{\chi}_h) \\ & = a_h(\boldsymbol{\Pi}_{\boldsymbol{h}}^{\boldsymbol{F}} \boldsymbol{\sigma} - \boldsymbol{\Pi}_k^0 \boldsymbol{\sigma}, \boldsymbol{\chi}_h) + a_h(\boldsymbol{\Pi}_k^0 \boldsymbol{\sigma}, \boldsymbol{\chi}_h) - (\mu(\boldsymbol{\sigma} - \boldsymbol{\Pi}_k^0 \boldsymbol{\sigma}), \boldsymbol{\chi}_h) - (\mu \boldsymbol{\Pi}_k^0 \boldsymbol{\sigma}, \boldsymbol{\chi}_h) \\ & \leq C(\|\boldsymbol{\sigma} - \boldsymbol{\Pi}_k^0 \boldsymbol{\sigma}\| + \|\boldsymbol{\Pi}_{\boldsymbol{h}}^{\boldsymbol{F}} \boldsymbol{\sigma} - \boldsymbol{\Pi}_k^0 \boldsymbol{\sigma}\| + h^{k+1} |\boldsymbol{\sigma}|_{k+1}) \|\boldsymbol{\chi}_h\| \text{ [By using (5) and (6)]} \\ & \leq Ch^{k+1} |\boldsymbol{\sigma}|_{k+1} \|\boldsymbol{\chi}_h\|. \end{aligned}$$

In a similar manner, one can address the solution of the second term on the right-hand side of equation (18) as:

$$\begin{aligned} & \int_0^t \mathcal{K}_h(t,s; \boldsymbol{\Pi}_{\boldsymbol{h}}^{\boldsymbol{F}} \boldsymbol{\sigma}(s), \boldsymbol{\chi}_h) ds - \int_0^t (\mathcal{K}(t,s) \boldsymbol{\sigma}(s), \boldsymbol{\chi}_h) ds \\ & \leq Ch^{k+1} \|\boldsymbol{\chi}_h\| \int_0^t |\boldsymbol{\sigma}(s)|_{k+1} ds. \end{aligned} \tag{20}$$

By using (13), (19), (20), $\boldsymbol{\Pi}_h^F$, $\|\nabla \cdot \boldsymbol{\psi}_h\| = 0$ and by considering $\boldsymbol{\chi}_h = \boldsymbol{\psi}_h$ in (18), we arrive at the following:

$$a_h(\boldsymbol{\psi}_h, \boldsymbol{\psi}_h) \leq Ch^{k+1} \left(|\boldsymbol{\sigma}|_{k+1} + \int_0^t |\boldsymbol{\sigma}(s)|_{k+1} ds \right) \|\boldsymbol{\psi}_h\| - \int_0^t \mathcal{K}_h(t,s; \boldsymbol{\psi}_h(s), \boldsymbol{\psi}_h) ds.$$

Use of boundedness of $\mathcal{K}_h(t,s;\cdot,\cdot)$ see [17], coercivity of $a_h(\boldsymbol{\psi}_h, \boldsymbol{\psi}_h)$ and (10), followed by Grönwall's lemma, yields:

$$\|\boldsymbol{\psi}_h\| \leq Ch^{k+1} \left(|\boldsymbol{\sigma}|_{k+1} + \int_0^t |\boldsymbol{\sigma}(s)|_{k+1} ds \right).$$

Now, the use of triangle inequality completes the proof of (16):

$$\|\boldsymbol{\vartheta}\| \leq Ch^{k+1} \left(|\boldsymbol{\sigma}|_{k+1} + \int_0^t |\boldsymbol{\sigma}(s)|_{k+1} ds \right). \tag{21}$$

To prove (17), we proceed by using the definition of mixed R.V. projection (13) as:

$$\begin{aligned}(\mu\boldsymbol{\vartheta},\boldsymbol{\chi}_h)+(\nabla\cdot\boldsymbol{\chi}_h,\tau_h)&=\mathcal{F}(\boldsymbol{\chi}_h)\quad\forall\boldsymbol{\chi}_h\in V_h^k,\\(\nabla\cdot\boldsymbol{\vartheta},\phi_h)&=0\quad\forall q_h\in Q_h^k,\end{aligned}\tag{22}$$

where

$$\begin{aligned}\mathcal{F}(\boldsymbol{\chi}_h)=&a_h(\tilde{\boldsymbol{\sigma}},\boldsymbol{\chi}_h)-(\mu\tilde{\boldsymbol{\sigma}},\boldsymbol{\chi}_h)+\int_0^t\mathcal{K}_h(t,s;\tilde{\boldsymbol{\sigma}}(s),\boldsymbol{\chi}_h)ds\\&-\int_0^t(\mathcal{K}(t,s)\boldsymbol{\sigma}(s),\boldsymbol{\chi}_h)ds.\end{aligned}\tag{23}$$

Let $\xi\in H^2(\mathcal{D})\cap H_0^1(\mathcal{D})$ be the solution of the dual problem:

$$-\nabla\cdot(a\nabla\xi)=\tau_h,\quad \xi=0\quad \text{on } \partial\mathcal{D},\tag{24}$$

and satisfy the following regularity condition:

$$\|\xi\|_2\le\|\tau_h\|.\tag{25}$$

Consider $\boldsymbol{\Phi}=a\nabla\xi$, then (24) will satisfy:

$$\begin{aligned}(\mu\boldsymbol{\Phi},\boldsymbol{\chi})+(\nabla\cdot\boldsymbol{\chi},\xi)&=0\quad\forall\boldsymbol{\chi}\in\mathcal{V},\\-(\nabla\cdot\boldsymbol{\Phi},\phi)&=(\tau_h,\phi)\quad\forall\phi\in\mathcal{Q}.\end{aligned}\tag{26}$$

Now, put $\phi=\tau_h$ in (26) to get:

$$\begin{aligned}\|\tau_h\|^2&=(\tau_h,-\nabla\cdot(\boldsymbol{\Pi}_h^F a\nabla\xi))\\&=(\mu\boldsymbol{\vartheta},\boldsymbol{\Pi}_h^F(a\nabla\xi))-\mathcal{F}(\boldsymbol{\Pi}_h^F(a\nabla\xi))\quad[\text{ By using (22) }].\end{aligned}\tag{27}$$

Now, from (23), we can rewrite $\mathcal{F}(\boldsymbol{\Pi}_h^F(a\nabla\xi))$ as:

(28)

$$\begin{aligned}&\mathcal{F}(\boldsymbol{\Pi}_h^F(a\nabla\xi))\\&=(a_h(\tilde{\boldsymbol{\sigma}}-\boldsymbol{\Pi}_k^0\boldsymbol{\sigma},\boldsymbol{\Pi}_h^F(a\nabla\xi))-(\mu(\tilde{\boldsymbol{\sigma}}-\boldsymbol{\Pi}_k^0\boldsymbol{\sigma}),\boldsymbol{\Pi}_h^F(a\nabla\xi)))\\&\quad+(a_h(\boldsymbol{\Pi}_k^0\boldsymbol{\sigma},\boldsymbol{\Pi}_h^F(a\nabla\xi))-(\mu\boldsymbol{\Pi}_k^0\boldsymbol{\sigma},\boldsymbol{\Pi}_h^F(a\nabla\xi)))-\left(\int_0^t(\mathcal{K}(t,s)(\boldsymbol{\vartheta})(s),\boldsymbol{\Pi}_h^F(a\nabla\xi))\right)\\&\quad+\left(\int_0^t\mathcal{K}_h(t,s;(\tilde{\boldsymbol{\sigma}}-\boldsymbol{\Pi}_k^0\boldsymbol{\sigma})(s),\boldsymbol{\Pi}_h^F(a\nabla\xi))ds\right.\\&\quad\left.-\int_0^t(\mathcal{K}(t,s)(\tilde{\boldsymbol{\sigma}}-\boldsymbol{\Pi}_k^0\boldsymbol{\sigma})(s),\boldsymbol{\Pi}_h^F(a\nabla\xi))\right)\\&\quad+\left(\int_0^t\mathcal{K}_h(t,s;\boldsymbol{\Pi}_k^0\boldsymbol{\sigma}(s),\boldsymbol{\Pi}_h^F(a\nabla\xi))ds-\int_0^t(\mathcal{K}(t,s)\boldsymbol{\Pi}_k^0\boldsymbol{\sigma}(s),\boldsymbol{\Pi}_h^F(a\nabla\xi))ds\right).\end{aligned}$$

The first and fourth terms on the right-hand side of (28) can be solved in a similar way as (12). We apply Lemma 1 to deal with the second and last terms whereas we use Cauchy-Schwarz inequality and (21) for the third term. Therefore, we arrive at the following:

$$\mathcal{F}(\boldsymbol{\Pi}_h^F(a\nabla\xi))\le Ch^{k+1}\left(|\boldsymbol{\sigma}|_{k+1}+\int_0^t|\boldsymbol{\sigma}(s)|_{k+1}ds\right)\|\xi\|_1,\tag{29}$$

whereas

$$(\mu\boldsymbol{\vartheta},\boldsymbol{\Pi}_h^F(a\nabla\xi))\le C\|\boldsymbol{\vartheta}\|\|\xi\|_1.\tag{30}$$

Using (29), (30), (21) and (25) in (27), we arrive at:

$$\|\tau_h\| \leq Ch^{k+1}\left(|\boldsymbol{\sigma}|_{k+1} + \int_0^t |\boldsymbol{\sigma}(s)|_{k+1}ds\right). \tag{31}$$

We get our desired estimates by using a triangle inequality and (5). □

3.2. Super Convergence property of τ_h. As evident from the equation (31), it is clear that τ_h exhibits convergence of order $O(h^{k+1})$. We can potentially enhance the convergence order of τ_h, by utilizing the dual norm approach, resulting in an order of $O(h^{k+2})$. This can be shown by rewriting (27) as:

$$\|\tau_h\|^2 = (\mu\boldsymbol{\vartheta}, \boldsymbol{\Pi_h^F}(a\nabla\xi) - a\nabla\xi) + (\nabla\cdot\boldsymbol{\vartheta}, \Pi_k^0\xi - \xi) - \mathcal{F}(\boldsymbol{\Pi_h^F}(a\nabla\xi)). \tag{32}$$

Now, by using (5) and (6) , we arrive at:

$$(\mu\boldsymbol{\vartheta}, \boldsymbol{\Pi_h^F}(a\nabla\xi) - a\nabla\xi) \leq Ch\|\boldsymbol{\vartheta}\|\|\xi\|_2, \tag{33}$$

$$(\nabla\cdot\boldsymbol{\vartheta}, \Pi_k^0\xi - \xi) \leq Ch^2\|\nabla\cdot\boldsymbol{\vartheta}\|\|\xi\|_2. \tag{34}$$

Now, (28), can be rewritten as:

$$\begin{aligned}
&\mathcal{F}(\boldsymbol{\Pi}_h^F(a\nabla\xi))\\
&= (a_h(\tilde{\boldsymbol{\sigma}} - \boldsymbol{\Pi}_k^0\boldsymbol{\sigma}, \boldsymbol{\Pi}_h^F(a\nabla\xi)) - (\mu(\tilde{\boldsymbol{\sigma}} - \boldsymbol{\Pi}_k^0\boldsymbol{\sigma}), \boldsymbol{\Pi}_h^F(a\nabla\xi)))\\
&\quad + (a_h(\boldsymbol{\Pi}_k^0\boldsymbol{\sigma}, \boldsymbol{\Pi}_h^F(a\nabla\xi)) - (\mu\boldsymbol{\Pi}_k^0\boldsymbol{\sigma}, \boldsymbol{\Pi}_h^F(a\nabla\xi)))\\
&\quad + \left(\int_0^t \mathcal{K}_h(t,s;(\tilde{\boldsymbol{\sigma}} - \boldsymbol{\Pi}_k^0\boldsymbol{\sigma})(s), \boldsymbol{\Pi}_h^F(a\nabla\xi))ds\right.\\
&\quad \left. - \int_0^t (\mathcal{K}(t,s)(\tilde{\boldsymbol{\sigma}} - \boldsymbol{\Pi}_k^0\boldsymbol{\sigma})(s), \boldsymbol{\Pi}_h^F(a\nabla\xi))\right)\\
&\quad + \left(\int_0^t \mathcal{K}_h(t,s;\boldsymbol{\Pi}_k^0\boldsymbol{\sigma}(s), \boldsymbol{\Pi}_h^F(a\nabla\xi))ds - \int_0^t (\mathcal{K}(t,s)\boldsymbol{\Pi}_k^0\boldsymbol{\sigma}(s), \boldsymbol{\Pi}_h^F(a\nabla\xi))ds\right)\\
&\quad - \int_0^t (\mathcal{K}(t,s)(\boldsymbol{\vartheta})(s), \boldsymbol{\Pi}_h^F(a\nabla\xi) - a\nabla\xi) - \int_0^t (\mathcal{K}(t,s)(\boldsymbol{\vartheta})(s), a\nabla\xi).
\end{aligned}$$

For the last term in the right-hand side of (35), we will use the dual norm approach, whereas all the remaining terms can be solved similarly to (28) by considering the higher regularity of ξ, i.e., $\|\xi\|_2$ as:

$$\mathcal{F}((\boldsymbol{\Pi}_h^F(a\nabla\xi)) \leq Ch^{k+2}\left(|\boldsymbol{\sigma}|_{k+1} + \int_0^t |\boldsymbol{\sigma}(s)|_{k+1}ds\right)\|\xi\|_2 + \int_0^t \|\boldsymbol{\vartheta}(s)\|_{-1}\|a\nabla\xi\|_1. \tag{35}$$

The term in the (33) can be bounded by using (21) and for (34), we proceed as:

$$\begin{aligned}
\|\nabla\cdot\boldsymbol{\vartheta}\|^2 &= (\nabla\cdot\boldsymbol{\vartheta}, \nabla\cdot(\boldsymbol{\sigma} - \boldsymbol{\Pi_h^F}\boldsymbol{\sigma}))\\
&\leq \|\nabla\cdot\boldsymbol{\vartheta}\|\|\nabla\cdot(\boldsymbol{\sigma} - \boldsymbol{\Pi_h^F}\boldsymbol{\sigma})\|\\
\Rightarrow \|\nabla\cdot\boldsymbol{\vartheta}\| &\leq Ch^k|\nabla\cdot\boldsymbol{\sigma}|_k.
\end{aligned} \tag{36}$$

For the estimate of $\|\boldsymbol{\vartheta}\|_{-1}$ in (35), let $\boldsymbol{\varkappa} \in (H^1(\mathcal{D}))^2$, then:

$$\begin{aligned}(\mu\boldsymbol{\vartheta}, \boldsymbol{\varkappa}) =& a_h(\tilde{\boldsymbol{\sigma}}, \boldsymbol{\Pi}_{\boldsymbol{k}}^{\mathbf{0}}\boldsymbol{\varkappa}) - (\mu\tilde{\boldsymbol{\sigma}}, \boldsymbol{\Pi}_{\boldsymbol{k}}^{\mathbf{0}}\boldsymbol{\varkappa}) \\ &+ \int_0^t \mathcal{K}_h(\tilde{\boldsymbol{\sigma}}(s), \boldsymbol{\Pi}_{\boldsymbol{k}}^{\mathbf{0}}\boldsymbol{\varkappa})ds - \int_0^t (\mathcal{K}\tilde{\boldsymbol{\sigma}}(s), \boldsymbol{\Pi}_{\boldsymbol{k}}^{\mathbf{0}}\boldsymbol{\varkappa})ds \\ &+ (\mu\boldsymbol{\vartheta}, \boldsymbol{\varkappa} - \boldsymbol{\Pi}_{\boldsymbol{k}}^{\mathbf{0}}\boldsymbol{\varkappa}) - \int_0^t (\mathcal{K}\boldsymbol{\vartheta}(s), \boldsymbol{\Pi}_{\boldsymbol{k}}^{\mathbf{0}}\boldsymbol{\varkappa})ds - (\nabla\cdot\boldsymbol{\Pi}_{\boldsymbol{k}}^{\mathbf{0}}\boldsymbol{\varkappa}, \tau_h).\end{aligned}$$

Solving all these terms and using Grönwall's lemma, we get the following:

$$\|\boldsymbol{\vartheta}\|_{-1} \leq Ch^{k+2}\left(|\boldsymbol{\sigma}|_{k+1} + \int_0^t |\boldsymbol{\sigma}(s)|_{k+1}ds\right) + \|\tau_h\|. \tag{37}$$

Using (37), (35), (34) and (36) in (32) followed by Grönwall's lemma:

$$\|\Pi_k^0 p - \tilde{p}\| \leq Ch^{k+2}\left(|\boldsymbol{\sigma}|_{k+1} + |\nabla\cdot\boldsymbol{\sigma}|_k + \int_0^t |\boldsymbol{\sigma}(s)|_{k+1}ds\right).$$

To prove the super convergence of $\Pi_k^0 p - p_h$, we must estimate $\Pi_k^0 p_t - \tilde{p}_t$. First we differentiate (13) and then follow the similar steps as above, we get the following:

$$\|\tau_{h,t}\| \leq Ch^{k+2}\left(|\boldsymbol{\sigma}_t|_{k+1} + |\nabla\cdot\boldsymbol{\sigma}_t|_k + |\boldsymbol{\sigma}|_{k+1} + \int_0^t (|\boldsymbol{\sigma}(s)|_{k+1} + |\nabla\cdot\boldsymbol{\sigma}(s)|_k)ds\right).$$

Lemma 2. *Under all the assumptions of Theorem 1 and $\boldsymbol{\sigma}_t, p_t \in X_\infty^{k+1}$, where p_t, $\boldsymbol{\sigma}_t$ and $\tilde{p}_t$, $\tilde{\boldsymbol{\sigma}}_t$ be the time derivative of p, $\boldsymbol{\sigma}$ and $\tilde{p}$, $\tilde{\boldsymbol{\sigma}}$ respectively, the following estimates hold true:*

$$\|\boldsymbol{\sigma}_t - \tilde{\boldsymbol{\sigma}}_t\|_{X_\infty^0} \leq Ch^{k+1}\left(|\boldsymbol{\sigma}_t|_{k+1} + |\boldsymbol{\sigma}|_{k+1} + \int_0^t |\boldsymbol{\sigma}(s)|_{k+1}ds\right),$$

$$\|p_t - \tilde{p}_t\|_{X_\infty^0} \leq Ch^{k+1}\left(|p_t|_{k+1} + |\boldsymbol{\sigma}_t|_{k+1} + |\boldsymbol{\sigma}|_{k+1} + \int_0^t |\boldsymbol{\sigma}(s)|_{k+1}ds\right).$$

Theorem 2. *Let p, $\boldsymbol{\sigma}$ and p_h, $\boldsymbol{\sigma}_h$ be the solution of continuous problem* (8) *and semi-discrete formulation* (9)*, respectively. Under all the assumptions of Lemma 2, the following estimates hold true:*

$$\|p - p_h\|_{X_\infty^0}^2 \leq C\left(\|\rho_h(\cdot,0)\|^2 + h^{2(k+1)}\left(|p|_{k+1}^2 + |\boldsymbol{\sigma}|_{k+1}^2 + \int_0^T g(s)ds\right)\right), \tag{38}$$

$$\|\boldsymbol{\sigma} - \boldsymbol{\sigma}_h\|_{X_\infty^0}^2 \leq C\left(|\boldsymbol{\vartheta}_h(\cdot,0)|^2 + Ch^{2(k+1)}\left(|\boldsymbol{\sigma}|_{k+1}^2 + \int_0^T g(s)ds\right)\right), \tag{39}$$

where $g(s) = |p_t(s)|_{k+1}^2 + |\boldsymbol{\sigma}_t(s)|_{k+1}^2 + |\boldsymbol{\sigma}(s)|_{k+1}^2$.

Proof. Writing $p - p_h = \rho + \rho_h$ and $\boldsymbol{\sigma} - \boldsymbol{\sigma}_h = \boldsymbol{\vartheta} + \boldsymbol{\vartheta}_h$ where $\rho_h = (\tilde{p} - p_h)$ and $\boldsymbol{\vartheta}_h = (\tilde{\boldsymbol{\sigma}} - \boldsymbol{\sigma}_h)$. Since, we already have the estimates of $\|\rho\|$ and $\|\boldsymbol{\vartheta}\|$, we need to find $\|\rho_h\|$ and $\|\boldsymbol{\vartheta}_h\|$. Use (8) and (9) to have the error equation as:

$$(p_t, \phi_h) - (p_{h,t}, \phi_h) - (\nabla\cdot(\boldsymbol{\sigma} - \boldsymbol{\sigma}_h), \phi_h) = 0 \quad \forall\phi_h \in Q_h^k, \tag{40}$$

$$\begin{aligned}(\mu\boldsymbol{\sigma}, \boldsymbol{\chi}_h) - a_h(\boldsymbol{\sigma}_h, \boldsymbol{\chi}_h) + \int_0^t [(\mathcal{K}(t,s)\boldsymbol{\sigma}(s), \boldsymbol{\chi}_h) - \mathcal{K}_h(t,s;\boldsymbol{\sigma}_h(s), \boldsymbol{\chi}_h)]ds \\ = (\nabla\cdot\boldsymbol{\chi}_h, p_h - p) \quad \forall\boldsymbol{\chi}_h \in V_h^k.\end{aligned} \tag{41}$$

Again rewrite (40) and (41) as:

$$(\rho_{h,t}, \phi_h) - (\nabla\cdot\boldsymbol{\vartheta}_h, \phi_h) = -(\rho_t, \phi_h), \tag{42}$$

$$a_h(\boldsymbol{\vartheta}_h, \boldsymbol{\chi}_h) + \int_0^t \mathcal{K}_h(t, s; \boldsymbol{\vartheta}_h(s), \boldsymbol{\chi}_h) ds + (\nabla \cdot \boldsymbol{\chi}_h, \rho_h) = 0. \tag{43}$$

Putting $\phi_h = \rho_h$ in (42) and $\boldsymbol{\chi}_h = \boldsymbol{\vartheta}_h$ in (43), then adding these equations, we get:

$$(\rho_{h,t}, \rho_h) + a_h(\boldsymbol{\vartheta}_h, \boldsymbol{\vartheta}_h) = -(\rho_t, \rho_h) - \int_0^t \mathcal{K}_h(t, s; \boldsymbol{\vartheta}_h(s), \boldsymbol{\vartheta}_h) ds.$$

By utilizing (10), along with the Cauchy-Schwarz inequality, Young's inequality, and employing the Kickback argument, we reach at the following result:

$$\frac{1}{2}\frac{d}{dt}\|\rho_h\|^2 + C_{\mu_1,\mathcal{K}'}\|\boldsymbol{\vartheta}_h\|^2 \leq C_\epsilon \|\rho_t\|^2 + C_{\epsilon'}\|\rho_h\|^2 + C_{\mathcal{K}} \int_0^t \|\boldsymbol{\vartheta}_h(s)\|^2 ds. \tag{44}$$

Integrating (44) from 0 to t, and then using Grönwall's lemma, we get:

$$\|\rho_h\|^2 + \int_0^t \|\boldsymbol{\vartheta}_h(s)\|^2 ds \leq C \left(\|\rho_h(\cdot, 0\|^2 + \int_0^t \|\rho_t(s)\|^2 ds \right)$$

$$\|\rho_h\|^2 \leq C \left(\|\rho_h(\cdot, 0)\|^2 + h^{2(k+1)} \int_0^t g(s) ds \right).$$

Now, using a triangle inequality and (17):

$$\|p - p_h\|^2 \leq C \left(\|\rho_h(\cdot, 0)\|^2 + h^{2(k+1)} \left(|p|_{k+1}^2 + |\boldsymbol{\sigma}|_{k+1}^2 + \int_0^t g(s) ds \right) \right).$$

For the proof of (39), differentiate (43), and then put $\boldsymbol{\chi}_h = \boldsymbol{\vartheta}_h$ and, $\phi_h = \rho_{h,t}$ in (42) to get:

$$\begin{aligned}
(\rho_{h,t}, \rho_{h,t}) + a_h(\boldsymbol{\vartheta}_{h,t}, \boldsymbol{\vartheta}_h) + \mathcal{K}_h(t, t; \boldsymbol{\vartheta}_h, \boldsymbol{\vartheta}_h) - \int_0^t k_{h,t}(t, s; \boldsymbol{\vartheta}_h(s), \boldsymbol{\vartheta}_h) ds \\
= -(\rho_t, \rho_{h,t})\|\rho_{h,t}\|^2 + \frac{\mu_1}{2}\frac{d}{dt}\|\boldsymbol{\vartheta}_h\|^2 \\
\leq C_{\mathcal{K}}\|\boldsymbol{\vartheta}_h\|^2 + C_{\mathcal{K}_t}\|\boldsymbol{\vartheta}_h\| \int_0^t \|\boldsymbol{\vartheta}_h(s)\| ds + C_\epsilon \|\rho_t\|^2 + C_{\epsilon'}\|\rho_{h,t}\|^2.
\end{aligned}$$

Using the Kickback argument followed by the integration from 0 to t, we arrive at the following:

$$\int_0^t \|\rho_{h,s}(s)\|^2 ds + \|\boldsymbol{\vartheta}_h\|^2 \leq C_1 \left(\|\boldsymbol{\vartheta}_h(\cdot, 0)\|^2 + \int_0^t \left(\|\boldsymbol{\vartheta}_h(s)\|^2 + \|\rho_t(s)\|^2 \right) ds \right).$$

Now, using Grönwall's lemma:

$$\|\boldsymbol{\vartheta}_h\|^2 \leq C \left(\|\boldsymbol{\vartheta}_h(\cdot, 0)\|^2 + \int_0^t \|\rho_t(s)\|^2 ds \right).$$

Using a triangle inequality and (16), we arrive at:

$$\|\boldsymbol{\sigma} - \boldsymbol{\sigma}_h\|^2 \leq C \left(\|\boldsymbol{\vartheta}_h(\cdot, 0)\|^2 + Ch^{2(k+1)} \left(|\boldsymbol{\sigma}|_{k+1}^2 + \int_0^t g(s) ds \right) \right).$$

□

Remark 2. *The estimate* (38) *and* (39) *involve the term* $\rho_h(\cdot, 0)$ *and* $\boldsymbol{\vartheta}_h(\cdot, 0)$ *respectively. We need to choose* $p_h(\cdot, 0)$ *and* $\boldsymbol{\sigma}_h(\cdot, 0)$ *in such a way that* $\rho_h(\cdot, 0)$ *and* $\boldsymbol{\vartheta}_h(\cdot, 0)$ *is of* $O(h^{k+1})$.

3.3. Super Convergence Analysis.

Theorem 3. *Let p and p_h be the solution of continuous problem* (8) *and semi-discrete formulation* (9)*, respectively. In accordance with all the presumptions outlined in Theorem 2, the following assertion remains valid:*

$$\|\Pi_k^0 p - p_h\|_{X_\infty^0} \leq O(h^{k+2}).$$

Proof. As shown in Section 3.2, the convergence of τ_h can be extended to $O(h^{k+2})$. Here we will analyze the super convergence properties of $\Pi_k^0 p - p_h$ by considering

$$\Pi_k^0 p - p_h = \Pi_k^0 p - \tilde{p} + \tilde{p} - p_h = \tau_h + \rho_h.$$

Since we know the estimate of τ_h (32) so our aim is to find the estimate for ρ_h and for that, we will proceed by using the fact that $\phi_h \in Q_h^k$ and $\nabla \cdot \boldsymbol{\chi}_h \in \mathbb{P}_k(E)$ and use the definition of Π_k^0 projection, we write (8) and (9)as:

$$(\Pi_k^0 p_t, \phi_h) - (p_{h,t}, \phi_h) - (\nabla \cdot (\boldsymbol{\sigma} - \boldsymbol{\sigma}_h), \phi_h) = 0 \quad \forall \phi_h \in Q_h^k, \tag{45}$$

$$\begin{aligned}(\mu\boldsymbol{\sigma}, \boldsymbol{\chi}_h) - a_h(\boldsymbol{\sigma}_h, \boldsymbol{\chi}_h) + \int_0^t [(\mathcal{K}(t,s)\boldsymbol{\sigma}(s), \boldsymbol{\chi}_h) - \mathcal{K}_h(t,s;\boldsymbol{\sigma}_h(s), \boldsymbol{\chi}_h)]ds \\ = (p_h - \Pi_k^0 p, \nabla \cdot \boldsymbol{\chi}_h) \quad \forall \boldsymbol{\chi}_h \in V_h^k.\end{aligned} \tag{46}$$

Rewriting (45) and (46) as:

$$(\delta_{h,t}, \phi_h) - (\nabla \cdot \boldsymbol{\vartheta}_h, \phi_h) = -(\Psi_{h,t}, \phi_h), \tag{47}$$

$$a_h(\boldsymbol{\vartheta}_h, \boldsymbol{\chi}_h) + \int_0^t \mathcal{K}_h(\boldsymbol{\vartheta}_h(s), \boldsymbol{\chi}_h)ds + (\nabla \cdot \boldsymbol{\chi}_h, \rho_h) = 0. \tag{48}$$

Put $\phi_h = \rho_h$ in (47) and $\boldsymbol{\chi}_h = \boldsymbol{\vartheta}_h$ in (48), followed by the similar steps as in Theorem 2, we get:

$$\begin{aligned}\|\rho_h\|^2 \leq & C\|\rho_h(\cdot,0)\|^2 \\ & + Ch^{2(k+2)} \int_0^t (|\boldsymbol{\sigma}_t(s)|_{k+1}^2 + |\nabla \cdot \boldsymbol{\sigma}_t(s)|_k^2 + |\nabla \cdot \boldsymbol{\sigma}(s)|_k^2 + |\boldsymbol{\sigma}(s)|_{k+1}^2)ds.\end{aligned}$$

□

4. Fully-Discrete Scheme

The error produced by a fully discrete scheme has two ingredients in theory: the error caused by spatial discretization, which is dependent on h, and the error caused by the time discretization, which is dependent on time phase size τ.
Now, we'll discretize our problem in time. To discretize in time, we use the Euler backward process. Divide the time interval into N distinct points that are evenly spaced, let $t_n = n\tau$ and the sequence $\{P_n\}$ and $\{\boldsymbol{\sigma}_n\}$ be generated as:

$$P_n \approx p_h(\cdot, t_n), \quad \boldsymbol{\sigma}_n \approx \boldsymbol{\sigma}_h(\cdot, t_n), \ \ n = 0, 1, 2, ..., N,$$

$$\tau = T/N.$$

Define $\bar{\partial}_t \Phi^n = \frac{\Phi(t_n) - \Phi(t_{n-1})}{\tau}$ and the left rectangular rule for the partitioning of the integral term for any function $\Phi(t)$ as:

$$\int_0^{t_n} \Phi(s)ds \approx \tau \sum_{j=0}^{n-1} \Phi(t_j).$$

Therefore, the fully discrete scheme is defined as:

$$\begin{aligned}&\left(\bar{\partial}_t P^n, \phi_h\right) - (\nabla\cdot\boldsymbol{\sigma}_n, \phi_h) = (f(t_n), \phi_h),\\ &a_h(\boldsymbol{\sigma}_n, \boldsymbol{\chi}_h) + \tau\sum_{j=0}^{n-1}\mathcal{K}_h(t_n, t_j; \boldsymbol{\sigma}_j, \boldsymbol{\chi}_h) + (\nabla\cdot\boldsymbol{\chi}_h, P_n) = 0.\end{aligned} \tag{49}$$

Theorem 4. *Let $p(\cdot, t_n)$ and P_n be the solution of continuous problem* (8) *and fully-discrete formulation* (49) *at time $t = t_n$ respectively. In accordance with all the presumptions outlined in Theorem 2 and $p_{tt} \in X_2^0$, the following assertion remains valid:*

$$\begin{aligned}&\|P_n - p(\cdot, t_n)\| \le O(h^{k+1} + \tau), \quad \forall n = 1, 2, \cdots, N,\\ &\|\boldsymbol{\sigma}_n - \boldsymbol{\sigma}(\cdot, t_n)\| \le O(h^{k+1} + \tau) \quad \forall n = 1, 2, \cdots, N.\end{aligned}$$

Proof. Let us write,

$$P_n - p(\cdot, t_n) = P_n - \tilde{p}(\cdot, t_n) + \tilde{p}(\cdot, t_n) - p(\cdot, t_n) = \rho_h^n + \rho^n,$$

$$\boldsymbol{\sigma}_n - \boldsymbol{\sigma}(\cdot, t_n) = \boldsymbol{\sigma}_n - \tilde{\boldsymbol{\sigma}}(\cdot, t_n) + \tilde{\boldsymbol{\sigma}}(\cdot, t_n) - \boldsymbol{\sigma}(\cdot, t_n) = \boldsymbol{\vartheta}_h^n + \boldsymbol{\vartheta}^n.$$

Since, we know the estimates for ρ^n and $\boldsymbol{\vartheta}^n$, we need to find $\|\rho_h^n\|$ and $\|\boldsymbol{\vartheta}_h^n\|$ and for that, we proceed by rewriting (49) and using (8) as:

$$\left(\bar{\partial}_t \rho_h^n, \phi_h\right) - (\nabla\cdot\boldsymbol{\vartheta}_h^n, \phi_h) = \left(p_t(\cdot, t_n) - \bar{\partial}_t\tilde{p}^n, \phi_h\right), \tag{50}$$

$$\begin{aligned}&a_h(\boldsymbol{\vartheta}_h^n, \boldsymbol{\chi}_h) + \tau\sum_{j=0}^{n-1}\mathcal{K}_h(t_n, t_j; \boldsymbol{\vartheta}_h^j, \boldsymbol{\chi}_h) + (\nabla\cdot\boldsymbol{\chi}_h, \rho_h^n)\\ &= (\nabla\cdot\boldsymbol{\chi}_h, p(\cdot, t_n) - \tilde{p}(\cdot, t_n))\\ &\quad + \int_0^{t_n}(\mathcal{K}(t, s)\boldsymbol{\sigma}(s), \boldsymbol{\chi}_h)ds - \tau\sum_{j=0}^{n-1}\mathcal{K}_h(t_n, t_j; \tilde{\boldsymbol{\sigma}}(\cdot, t_j), \boldsymbol{\chi}_h)\\ &\quad + (\mu\boldsymbol{\sigma}(\cdot, t_n), \boldsymbol{\chi}_h) - a_h(\tilde{\boldsymbol{\sigma}}(\cdot, t_n), \boldsymbol{\chi}_h).\end{aligned} \tag{51}$$

Add (50) and (51), after putting $\phi_h = \rho_h^n$ and $\boldsymbol{\chi}_h = \boldsymbol{\vartheta}_h^n$, and then use the definition of mixed Ritz Volterra projection to obtain:

$$\begin{aligned}&\left(\bar{\partial}_t\rho_h^n, \rho_h^n\right) + a_h(\boldsymbol{\vartheta}_h^n, \boldsymbol{\vartheta}_h^n) + \tau\sum_{j=0}^{n-1}\mathcal{K}_h(t_n, t_j; \boldsymbol{\vartheta}_h^j, \boldsymbol{\vartheta}_h^n)\\ &= \int_0^{t_n}\mathcal{K}_h(t_n, s; \tilde{\boldsymbol{\sigma}}(s), \boldsymbol{\vartheta}_h^n)ds - \tau\sum_{j=0}^{n-1}\mathcal{K}_h(t_n, t_j; \tilde{\boldsymbol{\sigma}}(\cdot, t_j), \boldsymbol{\vartheta}_h^n) + \left(p_t(\cdot, t_n) - \bar{\partial}_t\tilde{p}^n, \rho_h^n\right).\end{aligned}$$

Using (10) and boundedness of $\mathcal{K}_h(t_n, t_j; \cdot, \cdot)$, we arrive at:

$$\begin{aligned}&\frac{1}{2}\left(\frac{\|\rho_h^n\|^2 - \|\rho_h^{n-1}\|^2}{\tau} + \frac{\|\rho_h^n - \rho_h^{n-1}\|^2}{\tau}\right) + \mu_1\|\boldsymbol{\vartheta}_h^n\|^2\\ &\le (I_1^n, \rho_h^n) + (I_2^n, \boldsymbol{\vartheta}_h^n) + C\tau\sum_{j=0}^{n-1}\|\boldsymbol{\vartheta}_h^j\|\boldsymbol{\vartheta}_h^n\|,\end{aligned} \tag{52}$$

where

$$\begin{aligned}(I_1^n, \rho_h^n) &= \left(p_t(\cdot, t_n) - \bar{\partial}_t\tilde{p}^n, \rho_h^n\right)\\ &\le (\left\|p_t(\cdot, t_n) - \bar{\partial}_t p^n\right\| + \left\|\bar{\partial}_t p^n - \bar{\partial}_t\tilde{p}^n\right\|)\|\rho_h^n\|.\end{aligned}$$

(53)
$$(I_1^n, \rho_h^n) \leq C \left(\int_{t_{n-1}}^{t_n} \|p_{tt}(s)\| ds + \frac{h^{k+1}}{\tau} \int_{t_{n-1}}^{t_n} (|p_t(s)|_{k+1} + |\boldsymbol{\sigma}_t(s)|_{k+1} + |\boldsymbol{\sigma}(s)|_{k+1} + \int_0^s |\boldsymbol{\sigma}(z)|_{k+1} dz) ds \right) \|\rho_h^n\|.$$

where the term $(I_2^n, \boldsymbol{\vartheta}_h^n)$ can be solved as:

$$\begin{aligned}(I_2^n, \boldsymbol{\vartheta}_h^n) &= \int_0^{t_n} \mathcal{K}_h(t_n, s; \tilde{\boldsymbol{\sigma}}(s), \boldsymbol{\vartheta}_h^n) ds - \tau \sum_{j=0}^{n-1} \mathcal{K}_h(t_n, t_j; \tilde{\boldsymbol{\sigma}}(\cdot, t_j), \boldsymbol{\vartheta}_h^n) \\ &\leq C\tau \int_0^{t_n} \left| \frac{\partial}{\partial s} (\mathcal{K}_h(t_n, s; \tilde{\boldsymbol{\sigma}}(s), \boldsymbol{\vartheta}_h^n) ds \right| \\ &\leq C\tau \int_0^{t_n} (\|\tilde{\boldsymbol{\sigma}}(s) - \boldsymbol{\sigma}(s)\| + \|\boldsymbol{\sigma}(s)\| + \|\tilde{\boldsymbol{\sigma}}_t(s) - \boldsymbol{\sigma}_t(s)\| + \|\boldsymbol{\sigma}_t(s)\|) ds \|\boldsymbol{\vartheta}_h^n\|,\end{aligned}$$

and

(54)
$$(I_2^n, \boldsymbol{\vartheta}_h^n) \leq C\tau \int_0^{t_n} (\|\boldsymbol{\sigma}(s)\| + \|\boldsymbol{\sigma}_t(s)\| + h^{k+1}(|\boldsymbol{\sigma}(s)|_{k+1} + |\boldsymbol{\sigma}_t(s)|_{k+1} + \int_0^s |\boldsymbol{\sigma}(z)|_{k+1} dz)) ds \|\boldsymbol{\vartheta}_h^n\|.$$

Using (53) and (54) in (52), we get the following:

$$\begin{aligned}&\frac{1}{2} \left(\frac{\|\rho_h^n\|^2 - \|\rho_h^{n-1}\|^2}{\tau} \right) + \mu_1 \|\boldsymbol{\vartheta}_h^n\|^2 \\ &\leq C \left(\left(\tau \int_0^{t_n} (\|\boldsymbol{\sigma}(s)\| + \|\boldsymbol{\sigma}_t(s)\| + h^{k+1}(|\boldsymbol{\sigma}(s)|_{k+1} + |\boldsymbol{\sigma}_t(s)|_{k+1})) ds \right. \right. \\ &\quad \left. + \tau \sum_{j=0}^{n-1} \|\boldsymbol{\vartheta}_h^j\| \right) \|\boldsymbol{\vartheta}_h^n\| + \left(\int_{t_{n-1}}^{t_n} \|p_{tt}(s)\| ds + \frac{h^{k+1}}{\tau} \int_{t_{n-1}}^{t_n} (|p_t(s)|_{k+1} \right. \\ &\quad \left. \left. + |\boldsymbol{\sigma}_t(s)|_{k+1} + |\boldsymbol{\sigma}(s)|_{k+1} + \int_0^s |\boldsymbol{\sigma}(z)|_{k+1} dz) ds \right) \|\rho_h^n\| \right).\end{aligned}$$

Applying Young's inequality and subsequently employing the Kickback argument leads us to the following:

(55)
$$\begin{aligned}&\frac{1}{2} \left(\frac{\|\rho_h^n\|^2 - \|\rho_h^{n-1}\|^2}{\tau} \right) + C_1 \|\boldsymbol{\vartheta}_h^n\|^2 \\ &\leq C_2 \left(\tau \sum_{j=0}^{n-1} \|\boldsymbol{\vartheta}_h^j\|^2 + \|\rho_h^n\|^2 + \tau \int_{t_{n-1}}^{t_n} \|p_{tt}(s)\|^2 ds. \right. \\ &\quad + \tau^2 \int_0^{t_n} (\|\boldsymbol{\sigma}(s)\|^2 + \|\boldsymbol{\sigma}_t(s)\|^2 + h^{2(k+1)}(|\boldsymbol{\sigma}(s)|_{k+1}^2 + |\boldsymbol{\sigma}_t(s)|_{k+1}^2)) ds \\ &\quad \left. + \frac{h^{2(k+1)}}{\tau} \int_{t_{n-1}}^{t_n} \left(g(s) + \int_0^s |\boldsymbol{\sigma}(z)|_{k+1}^2 dz \right) ds \right).\end{aligned}$$

Multiplying (55) by 2τ and summing from 1 to m, with $1 \leq m \leq N$ gives:

$$\begin{aligned}
&\|\rho_h^m\|^2 + 2\tau C_1 \sum_{n=1}^{m} \|\boldsymbol{\vartheta}_h^n\|^2 \\
&\leq \|\rho(\cdot,0)\|^2 + 2C_2 \left(\tau^2 \sum_{n=1}^{m} \sum_{j=0}^{n-1} \|\boldsymbol{\vartheta}_h^j\|^2 + \tau \sum_{n=1}^{m} \|\rho_h^n\|^2 \right. \\
&\quad + \tau^2 \int_0^T (\|\boldsymbol{\sigma}(s)\|^2 + \|\boldsymbol{\sigma}_t(s)\|^2) ds + \tau^2 \int_0^T \|p_{tt}(s)\|^2 ds \\
&\quad \left. + h^{2(k+1)} \int_0^T g(s) ds + \tau^2 h^{2(k+1)} \int_0^T (|\boldsymbol{\sigma}(s)|_{k+1}^2 + |\boldsymbol{\sigma}_t(s)|_{k+1}^2) ds \right).
\end{aligned}$$

Using Grönwall's lemma and replacing m by n, we get our desired result:

$$\|\rho_h^n\| \leq O(h^{k+1} + \tau).$$

For the estimate of $\boldsymbol{\vartheta}_h^n$, we proceed by rewriting (51) as:

$$\begin{aligned}
&a_h(\boldsymbol{\vartheta}_h^n, \boldsymbol{\chi}_h) + \tau \sum_{j=0}^{n-1} \mathcal{K}_h(t_n, t_j; \boldsymbol{\vartheta}_h^j, \boldsymbol{\chi}_h) + (\nabla \cdot \boldsymbol{\chi}_h, \rho_h^n) \\
&= \int_0^{t_n} \mathcal{K}_h(t_n, s; \tilde{\boldsymbol{\sigma}}(s), \boldsymbol{\chi}_h) ds - \tau \sum_{j=0}^{n-1} \mathcal{K}_h(t_n, t_j; \tilde{\boldsymbol{\sigma}}(t_j), \boldsymbol{\chi}_h).
\end{aligned} \tag{56}$$

Again considering (56) at time step $t = t_{n-1}$, we obtain:

$$\begin{aligned}
&a_h(\boldsymbol{\vartheta}_h^{n-1}, \boldsymbol{\chi}_h) + \tau \sum_{j=0}^{n-2} \mathcal{K}_h(t_{n-1}, t_j; \boldsymbol{\vartheta}_h^j, \boldsymbol{\chi}_h) + (\nabla \cdot \boldsymbol{\chi}_h, \rho_h^{n-1}) \\
&= \int_0^{t_{n-1}} \mathcal{K}_h(t_{n-1}, s; \tilde{\boldsymbol{\sigma}}(s), \boldsymbol{\chi}_h) ds - \tau \sum_{j=0}^{n-2} \mathcal{K}_h(t_{n-1}, t_j; \tilde{\boldsymbol{\sigma}}(t_j), \boldsymbol{\chi}_h).
\end{aligned} \tag{57}$$

Now, subtracting (57) from(56), and then dividing by τ, we arrive at:

$$\begin{aligned}
&a_h\left(\bar{\partial}_t \boldsymbol{\vartheta}_h^n, \boldsymbol{\chi}_h\right) + \sum_{j=0}^{n-1} \mathcal{K}_h(t_n, t_j; \boldsymbol{\vartheta}_h^j, \boldsymbol{\chi}_h) \\
&- \sum_{j=0}^{n-2} \mathcal{K}_h(t_{n-1}, t_j; \boldsymbol{\vartheta}_h^j, \boldsymbol{\chi}_h) + \left(\nabla \cdot \boldsymbol{\chi}_h, \bar{\partial}_t \rho_h^n\right) \\
&= \frac{1}{\tau} \left(\int_0^{t_n} \mathcal{K}_h(t_n, s; \tilde{\boldsymbol{\sigma}}(s), \boldsymbol{\chi}_h) ds - \tau \sum_{j=0}^{n-1} \mathcal{K}_h(t_n, t_j; \tilde{\boldsymbol{\sigma}}(t_j), \boldsymbol{\chi}_h) \right) \\
&\quad - \frac{1}{\tau} \left(\int_0^{t_{n-1}} \mathcal{K}_h(t_{n-1}, s; \tilde{\boldsymbol{\sigma}}(s), \boldsymbol{\chi}_h) ds - \tau \sum_{j=0}^{n-2} \mathcal{K}_h(t_{n-1}, t_j; \tilde{\boldsymbol{\sigma}}(t_j), \boldsymbol{\chi}_h) \right).
\end{aligned} \tag{58}$$

Put $\phi_h = \bar{\partial}_t \rho_h^n$ in (50) and $\boldsymbol{\chi}_h = \boldsymbol{\vartheta}_h^n$ in (58) and then add, we obtain:

$$\begin{aligned}
&\|\bar{\partial}_t \rho_h^n\|^2 + a_h\left(\bar{\partial}_t \boldsymbol{\vartheta}_h^n, \boldsymbol{\vartheta}_h^n\right) + \sum_{j=0}^{n-1} \mathcal{K}_h(t_n, t_j; \boldsymbol{\vartheta}_h^j, \boldsymbol{\vartheta}_h^n) - \sum_{j=0}^{n-2} \mathcal{K}_h(t_{n-1}, t_j; \boldsymbol{\vartheta}_h^j, \boldsymbol{\vartheta}_h^n) \\
&= \left(p_t(\cdot, t_n) - \bar{\partial}_t \tilde{p}^n, \bar{\partial}_t \rho_h^n\right) \\
&\quad + \frac{1}{\tau}\left(\int_0^{t_n} \mathcal{K}_h(t_n, s; \tilde{\boldsymbol{\sigma}}(s), \boldsymbol{\vartheta}_h^n) ds - \tau \sum_{j=0}^{n-1} \mathcal{K}_h(t_n, t_j; \tilde{\boldsymbol{\sigma}}(t_j), \boldsymbol{\vartheta}_h^n)\right) \\
&\quad - \frac{1}{\tau}\left(\int_0^{t_{n-1}} \mathcal{K}_h(t_{n-1}, s; \tilde{\boldsymbol{\sigma}}(s), \boldsymbol{\vartheta}_h^n) ds - \tau \sum_{j=0}^{n-2} \mathcal{K}_h(t_{n-1}, t_j; \tilde{\boldsymbol{\sigma}}(t_j), \boldsymbol{\vartheta}_h^n)\right)
\end{aligned}$$

and

$$\begin{aligned}
&\|\bar{\partial}_t \rho_h^n\|^2 + a_h\left(\bar{\partial}_t \boldsymbol{\vartheta}_h^n, \boldsymbol{\vartheta}_h^n\right) + \sum_{j=0}^{n-1} \mathcal{K}_h(t_n, t_j; \boldsymbol{\vartheta}_h^j, \boldsymbol{\vartheta}_h^n) - \sum_{j=0}^{n-2} \mathcal{K}_h(t_{n-1}, t_j; \boldsymbol{\vartheta}_h^j, \boldsymbol{\vartheta}_h^n) \\
&= (I_1^n, \bar{\partial}_t \rho_h^n) + \frac{1}{\tau}(I_3^n, \boldsymbol{\vartheta}_h^n), \qquad (59)
\end{aligned}$$

where

$$\begin{aligned}
(I_1^n, \bar{\partial}_t \rho_h^n) &\le C_\epsilon \left(\tau \int_{t_{n-1}}^{t_n} \|p_{tt}(s)\|^2 ds + \frac{h^{2k+2}}{\tau} \int_{t_{n-1}}^{t_n} \left(g(s) + \int_0^s |\boldsymbol{\sigma}(z)|_{k+1}^2 dz\right) ds\right) \\
&\quad + C_{\epsilon'} \|\bar{\partial}_t \rho_h^n\|^2, \qquad (60)
\end{aligned}$$

and

$$\begin{aligned}
(I_3^n, \boldsymbol{\vartheta}_h^n) &= \left(\int_0^{t_n} \mathcal{K}_h(t_n, s; \tilde{\boldsymbol{\sigma}}(s), \boldsymbol{\vartheta}_h^n) ds - \tau \sum_{j=0}^{n-1} \mathcal{K}_h(t_n, t_j; \tilde{\boldsymbol{\sigma}}(t_j), \boldsymbol{\vartheta}_h^n)\right) \\
&\quad - \left(\int_0^{t_{n-1}} \mathcal{K}_h(t_{n-1}, s; \tilde{\boldsymbol{\sigma}}(s), \boldsymbol{\vartheta}_h^n) ds - \tau \sum_{j=0}^{n-2} \mathcal{K}_h(t_{n-1}, t_j; \tilde{\boldsymbol{\sigma}}(t_j), \boldsymbol{\vartheta}_h^n)\right) \\
&= \int_0^{t_{n-1}} \left(\mathcal{K}_h(t_n, s; \tilde{\boldsymbol{\sigma}}(s), \boldsymbol{\vartheta}_h^n) - \mathcal{K}_h(t_{n-1}, s; \tilde{\boldsymbol{\sigma}}(s), \boldsymbol{\vartheta}_h^n)\right) ds \\
&\quad - \tau \sum_{j=0}^{n-2} \left(\mathcal{K}_h(t_n, t_j; \tilde{\boldsymbol{\sigma}}(t_j), \boldsymbol{\vartheta}_h^n) - \mathcal{K}_h(t_{n-1}, t_j; \tilde{\boldsymbol{\sigma}}(t_j), \boldsymbol{\vartheta}_h^n)\right) \\
&\quad + \int_{t_{n-1}}^{t_n} \mathcal{K}_h(t_n, s; \tilde{\boldsymbol{\sigma}}(s), \boldsymbol{\vartheta}_h^n) ds - \tau \mathcal{K}_h(t_n, t_{n-1}, \tilde{\boldsymbol{\sigma}}(t_{n-1}), \boldsymbol{\vartheta}_h^n) \\
(I_3^n, \boldsymbol{\vartheta}_h^n) &\le \tau^2 \int_0^{t_{n-1}} \left|\frac{\partial}{\partial s}\left(\mathcal{K}_{h,t}(t_{n^*}, s; \tilde{\boldsymbol{\sigma}}(s), \boldsymbol{\vartheta}_h^n)\right)\right| ds \\
&\quad + \tau \int_{t_{n-1}}^{t_n} \left|\frac{\partial}{\partial s}\left(\mathcal{K}_h(t, s; \tilde{\boldsymbol{\sigma}}(s), \boldsymbol{\vartheta}_h^n)\right)\right| ds,
\end{aligned}$$

where $t_{n^*} \in (t_{n-1}, t_n)$.

(61)

$$\begin{aligned}
&\frac{1}{\tau}(I_3^n, \boldsymbol{\vartheta}_h^n)\\
\leq&\tau \int_0^{t_{n-1}} \left| \frac{\partial}{ds}(\mathcal{K}_{h,t}(t_{n^*}, s; \tilde{\boldsymbol{\sigma}}(s), \boldsymbol{\vartheta}_h^n)) \right| ds + \int_{t_{n-1}}^{t_n} \left| \frac{\partial}{ds}(\mathcal{K}_h(t, s; \tilde{\boldsymbol{\sigma}}(s), \boldsymbol{\vartheta}_h^n)) \right| ds\\
\leq& C \left(\tau^2 \int_0^{t_{n-1}} (\|\boldsymbol{\sigma}(s)\|^2 + \|\boldsymbol{\sigma}_t(s)\|^2) ds + \tau \int_{t_{n-1}}^{t_n} (\|\boldsymbol{\sigma}(s)\|^2 + \|\boldsymbol{\sigma}_t(s)\|^2) ds \right.\\
&+ \tau^2 h^{2(k+1)} \int_0^{t_{n-1}} \left(|\boldsymbol{\sigma}(s)|_{k+1}^2 + |\boldsymbol{\sigma}_t(s)|_{k+1}^2 + \int_0^s |\boldsymbol{\sigma}(z)|_{k+1}^2 dz \right) ds\\
&\left. + \tau h^{2(k+1)} \int_{t_{n-1}}^{t_n} \left(|\boldsymbol{\sigma}(s)|_{k+1}^2 + |\boldsymbol{\sigma}_t(s)|_{k+1}^2 + \int_0^s |\boldsymbol{\sigma}(z)|_{k+1}^2 dz \right) ds + \|\boldsymbol{\vartheta}_h^n\|^2 \right).
\end{aligned}$$

Put (60) and (61) in (59), to arrive at:

(62)

$$\begin{aligned}
&\|\bar{\partial}_t \rho_h^n\|^2 + \mu_1 \left(\frac{\|\boldsymbol{\vartheta}_h^n\|^2 - \|\boldsymbol{\vartheta}_h^{n-1}\|^2}{2\tau} \right)\\
\leq& -\tau \sum_{j=0}^{n-2} \mathcal{K}_{h,t}(t_{n^*}, t_j; \boldsymbol{\vartheta}_h^j, \boldsymbol{\vartheta}_h^n) - \mathcal{K}_h(t_n, t_{n-1}; \boldsymbol{\vartheta}_h^{n-1}, \boldsymbol{\vartheta}_h^n) + C \left(\|\bar{\partial}_t \rho_h^n\|^2 + \|\boldsymbol{\vartheta}_h^n\|^2 \right.\\
&+ \frac{h^{2k+2}}{\tau} \int_{t_{n-1}}^{t_n} \left(g(s) + \int_0^s \|\boldsymbol{\sigma}(z)\|_{k+1}^2 dz \right) ds\\
&+ \tau^2 \int_0^{t_{n-1}} (\|\boldsymbol{\sigma}(s)\|^2 + \|\boldsymbol{\sigma}_t(s)\|^2) ds + \tau \int_{t_{n-1}}^{t_n} (\|\boldsymbol{\sigma}(s)\|^2 + \|\boldsymbol{\sigma}_t(s)\|^2) ds\\
&+ \tau^2 h^{2(k+1)} \int_0^{t_{n-1}} \left(|\boldsymbol{\sigma}(s)|_{k+1}^2 + |\boldsymbol{\sigma}_t(s)|_{k+1}^2 + \int_0^s |\boldsymbol{\sigma}(z)|_{k+1}^2 dz \right) ds\\
&\left. + \tau \int_{t_{n-1}}^{t_n} \left(\|p_{tt}(s)\|^2 + h^{2(k+1)} \left(|\boldsymbol{\sigma}(s)|_{k+1}^2 + |\boldsymbol{\sigma}_t(s)|_{k+1}^2 + \int_0^s |\boldsymbol{\sigma}(z)|_{k+1}^2 dz \right) \right) ds \right).
\end{aligned}$$

Multiplying (62) by 2τ, using kickback argument and then summing from $n = 1$ to m, we obtain:

$$\begin{aligned}
\|\boldsymbol{\vartheta}_h^m\|^2 \leq& C_1 \tau \sum_{n=1}^{m} \|\boldsymbol{\vartheta}_h^n\|^2 + C_2 \left(\tau^2 \int_0^T (\|p_{tt}(s)\|^2 + \|\boldsymbol{\sigma}(s)\|^2 + \|\boldsymbol{\sigma}_t(s)\|^2) ds \right.\\
&\left. + \|\vartheta_h(\cdot, 0)\|^2 + h^{2k+2} \int_0^T g(s) ds \right).
\end{aligned}$$

By using Grönwall's lemma, we may replace m by n to get our desired estimate:

$$\|\boldsymbol{\vartheta}_h^n\| \leq O(h^{k+1} + \tau).$$

□

5. Numerical Results

Within this section, we are set to conduct numerical experiments aimed at validating the effectiveness of the introduced mixed virtual element scheme for the

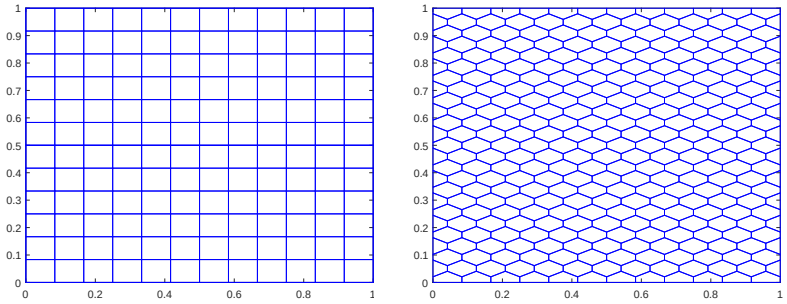

FIGURE 1. An illustration of polygonal meshes: on the left $\mathcal{Q}_{1/12}$, and on the right, $\mathcal{H}_{1/12}$.

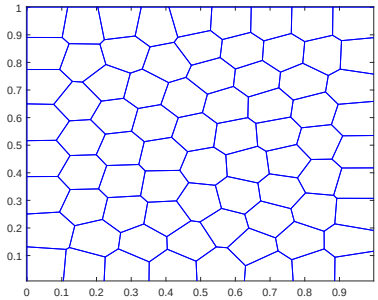

FIGURE 2. An illustration of Voronoi mesh $\mathcal{V}_{1/6}$.

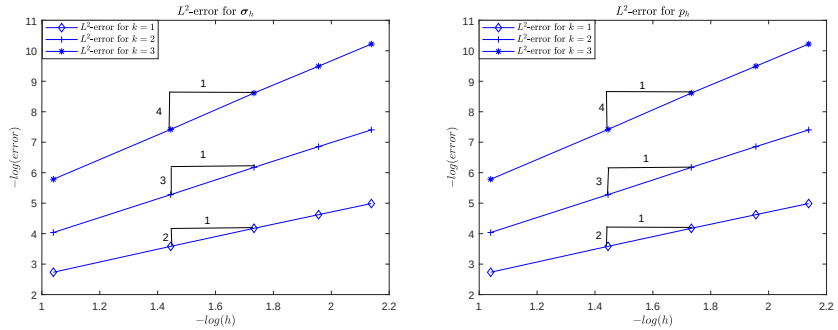

FIGURE 3. Order of convergence for Example 1 on the quadrilateral mesh.

PIDE (1). Our investigation encompasses distinct mesh types: a quadrilateral mesh, a hexagonal mesh, voronoi mesh as illustrated in Figure 1 and Figure 2. Here, we consider the domain $\mathcal{D}$ the unit square in $\mathbb{R}^2$. Before presenting the numerical results, it is important for us to have a better understanding of both the spaces, dofs, and how bilinear forms can be computed on these spaces. All the discrete forms are already explained in Section-2.2. In (49) the bilinear forms (P_n, ϕ_h) and $(f(t_n), \phi_h)$ involves multiplication with polynomials so, can be done by using

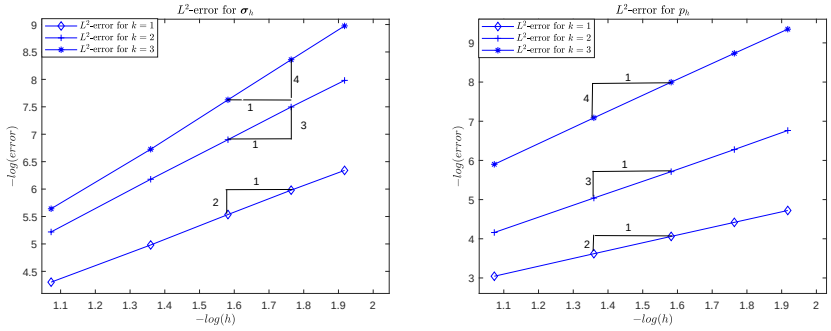

FIGURE 4. Order of convergence for Example 1 on the hexagonal mesh.

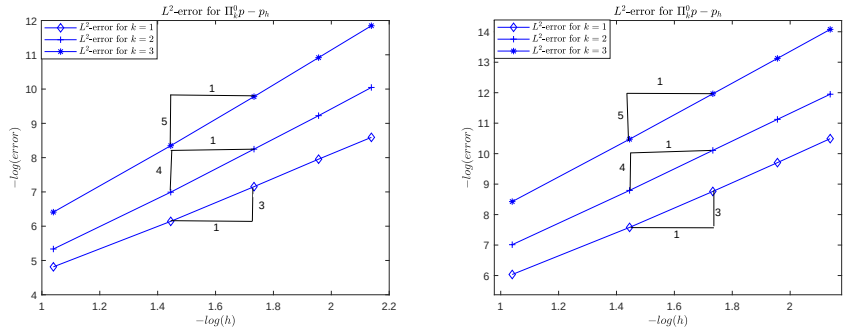

FIGURE 5. Order of convergence for $\Pi_k^0 p - p_h$ on the quadrilateral mesh. The left-hand panel pertains to Example 1, while the right-hand panel pertains to Example 2.

any quadrature rule of appropriate order, whereas for the discrete forms $a_h^E(\cdot,\cdot)$, $\mathcal{K}_h^E(\cdot,\cdot)$ and $(\nabla\cdot\boldsymbol{\sigma}_n, \phi_h)_E$, dofs of $V_h^k(E)$ will be needed (as defined in section-2.1). For more details about the implementation, we refer to [5].

We use the backward Euler approach for time discretization coupled with mixed VEM discretization to tackle the fully discrete problem, for the polygonal mesh sequences.

Example 1 Consider the linear PIDE (1), with coefficients $a(x) = x$, $b(x;t,s) = xe^{(t-s)}$, exact solution $p(x,t) = t\sin(2\pi x)\sin(2\pi y)$ whereas $\mathcal{K}(x;t,s) = \frac{e^{2(t-s)}}{x}$. Notably, the load term f, boundary data, and initial data u_0 are all determined using the exact solution as a reference point.

Example 2 Consider the linear PIDE (1), with cofficients $a(x) = x$, $b(x;t,s) = x\left(\frac{2+\cos(s)}{2+\cos(t)}\right)$, exact solution $p(x,t) = te^{x+t}(x-x^2)\sin(2\pi y)$ whereas $\mathcal{K}(x;t,s) = \left(\frac{2+\cos(s)}{x(2+\cos(t))}\right)e^{(t-s)}$. Notably, the load term f, boundary data, and initial data u_0 are all determined using the exact solution as a reference point.

Example 3 Consider the linear PIDE (1), with coefficients $a(x) = 1$, $b(x;t,s) = ts$, exact solution $p(x,t) = t(x-x^2)(y-y^2)$. Here $\mathcal{K}(x;t,s)$ is approximated by the first

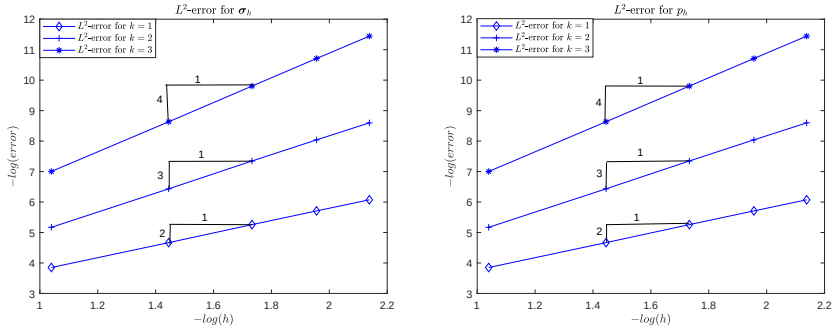

FIGURE 6. Order of convergence for Example 2 on the quadrilateral mesh.

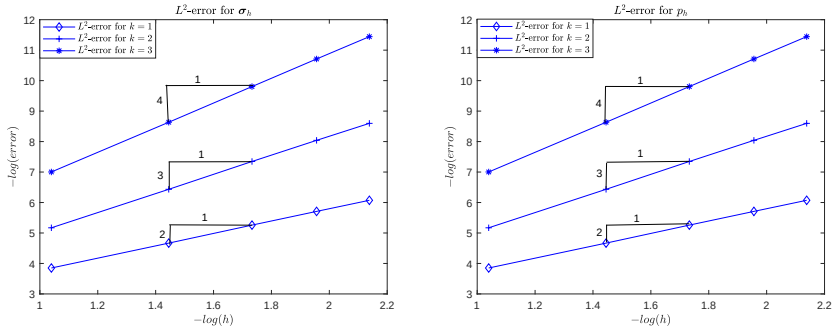

FIGURE 7. Order of convergence for Example 3 on the quadrilateral mesh in case of k=1, 2 and 3.

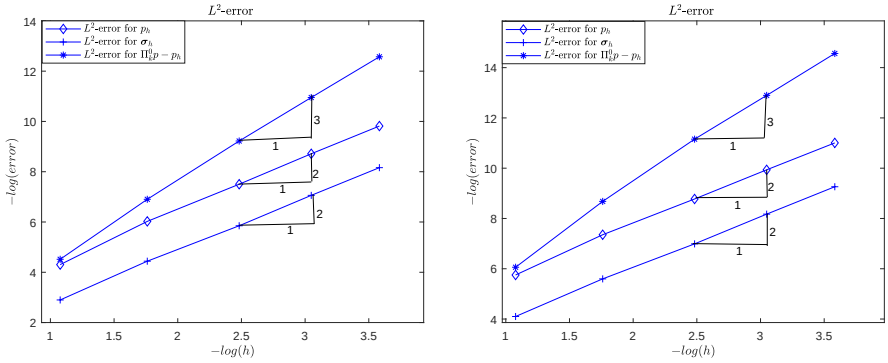

FIGURE 8. Order of convergence for Example 1 and Example 2 on the Voronoi mesh in case of k=1.

five terms of the series generated using (7). Notably, the load term f, boundary data, and initial data u_0 are all determined using the exact solution as a reference point.

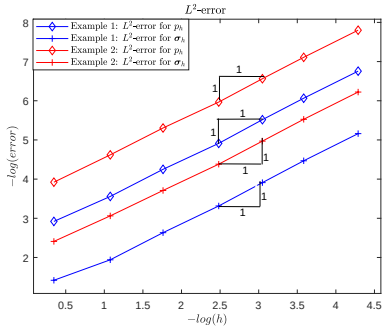

FIGURE 9. Order of convergence for Example 1 and Example 2 on the Voronoi mesh in case of k=0.

Below, we present a numerical example showing that even if we don't know the explicit form of a resolvent kernel our formulation still works by truncating the series of resolvent kernel after a few steps. In the example presented below, the resolvent kernel comes out to be in a series so here, we have considered the first five terms of the resolvent kernel and find out that numerical results are still in accordance with the theoretical results.

Fig. 3 and 4 depict the order of convergence for both p_h and $\boldsymbol{\sigma}_h$ for Example 1 in case of $k = 1, 2$ and 3 on quadrilateral and hexagonal mesh respectively. Both the figures show that these orders of convergence are accomplished in perfect accordance with theory while Fig. 5 shows the super convergence results for both Example 1 and Example 2 in the case of k= 1, 2, and 3 on the quadrilateral mesh whereas in Fig 6 shows the order of convergence for Example 2 on the quadrilateral mesh. Fig 7 shows the convergence corresponding to Example 3. Figure 8 displays the convergence of Example 1 and Example 2 on the Voronoi mesh. From all the figures and Table, we can see that our theory is well according to our numerical results.

Remark 3. *From Remark 6.3 of* [8]*, we can see that the lowest order Raviart Thomas element can be constructed for* $k = 0$ *with the usual convention* $\mathbb{P}_{-1}(E) = 0$.

Remark 4. *Whenever we are unable to find the explicit form of the resolvent kernel, we can use the first few terms of the series to achieve the optimal order of convergence, as shown in example 3.*

6. Conclusions

Considering the advantages of VEM and mixed methods, we applied a mixed VEM approach to address both the semi-discrete and fully-discrete schemes to solve the PIDE (1). In this article, we have introduced a novel projection known as mixed R.V. projection, which helps in handling the integral term. The semi-discrete scheme and error estimates presented in this work align with those obtained in the previous study [18]. This research marks a significant contribution to the literature [35, 17, 18] only with semidiscrete formulation while here, we represent the first comprehensive examination of the fully discrete scheme within this formulation. Furthermore, a step-by-step analysis is proposed for the super convergence of the discrete solution of order $O(h^{k+2})$. Several computational experiments are

discussed to validate the proposed schemes computational efficiency and support the theoretical conclusions.

Acknowledgments

The first author acknowledges the financial support provided by CSIR through grant 1044/(CSIR-UGC NET DEC.2018). The second author expresses gratitude towards the Department of Science and Technology (DST-SERB) in India for their backing under grant number CRG/2020/001599.

References

[1] Beirão da Veiga, L., Brezzi, F., Cangiani, A., Manzini, G., Marini, L.D. and Russo, A., Basic principles of virtual element methods, Mathematical Models and Methods in Applied Sciences, 23(01), 199-214, 2013.

[2] Beirão da Veiga, L., Brezzi, F., Marini, L.D. and Russo, A., The hitchhiker's guide to the virtual element method, Mathematical Models and Methods in Applied Sciences, 24(08), 1541-1573, 2014.

[3] Beirão da Veiga, L., Brezzi, F., Marini, L.D. and Russo, A., H(div) and H(curl)-conforming virtual element methods, Numerische Mathematik, 133, 303-332, 2016.

[4] Beirão da Veiga, L., Brezzi, F., Marini, L.D. and Russo, A., Mixed virtual element methods for general second order elliptic problems on polygonal meshes, ESAIM: Mathematical Modelling and Numerical Analysis, 50(3), 727-747, 2016.

[5] Beirão da Veiga, L., Brezzi, F., Marini, L.D. and Russo, A., Virtual element implementation for general elliptic equations, Building Bridges: Connections and Challenges in Modern Approaches to Numerical Partial Differential Equations, 39-71, 2016.

[6] Beirão da Veiga, L., Brezzi, F., Marini, L.D. and Russo, A., Virtual element method for general second-order elliptic problems on polygonal meshes, Mathematical Models and Methods in Applied Sciences, 26(04), 729-750, 2016.

[7] Brenner, S.C. and Sung, L.Y., Virtual element methods on meshes with small edges or faces, Mathematical Models and Methods in Applied Sciences, 28(07), 1291-1336, 2018.

[8] Brezzi, F., Falk, R.S. and Marini, L.D., Basic principles of mixed virtual element methods, ESAIM: Mathematical Modelling and Numerical Analysis, 48(4), 1227-1240, 2014.

[9] Càceres E. and Gatica, G.N., A mixed virtual element method for the pseudostressvelocity formulation of the Stokes problem, IMA Journal of Numerical Analysis, 37(1), 296-331, 2017.

[10] Càceres, E., Gatica, G.N. and Sequeira, F.A., A mixed virtual element method for the Brinkman problem, Mathematical Models and Methods in Applied Sciences, 27(04), 707-743, 2017.

[11] Càceres, E., Gatica, G.N. and Sequeira, F.A., A mixed virtual element method for quasi-Newtonian Stokes flows, SIAM Journal on Numerical Analysis, 56(1), 317-343, 2018.

[12] Cannon, J.R. and Lin, Y., A priori L^2 error estimates for finite-element methods for nonlinear diffusion equations with memory, SIAM Journal on Numerical Analysis, 27(3), 595-607, 1990.

[13] Cao, S. and Chen, L., Anisotropic error estimates of the linear virtual element method on polygonal meshes, SIAM Journal on Numerical Analysis, 56(5), 2913-2939, 2018.

[14] Deka, B. and Deka, R.C., A priori $L^\infty(L^2)$ error estimates for finite element approximations to parabolic integro-differential equations with discontinuous coefficients, Proceedings of The Indian Academy Of Science-Mathematical Sciences, Springer India, 129(4), 1-20, 2019.

[15] Evans, L.C., Partial differential equations American Mathematical Society, 19, 2022.

[16] Ewing, R.E., Lazarov, R.D. and Lin, Y., Finite volume element approximations of integro-differential parabolic problems, Recent Advances in Numerical Methods and Applications II, 3-15 1999.

[17] Ewing, R.E., Lin, Y. and Wang, J., A numerical approximation of non-Fickian flows with mixing length growth in porous media, Acta Mathematica Universitatis Comenianae, New Series, 70(1), 75-84, 2001.

[18] Ewing, R.E., Lin, Y., Sun, T., Wang, J. and Zhang, S., Sharp L^2-error estimates and superconvergence of mixed finite element methods for non-Fickian flows in porous media, SIAM Journal On Numerical Analysis, 40(4), 1538-1560, 2002.

[19] Fakhar-Izadi, F. and Dehghan, M., Space-time spectral method for a weakly singular parabolic partial integro-differential equation on irregular domains, Computers & Mathematics with Applications, 67(10), 1884-1904, 2014.

[20] Fakhar-Izadi, F. and Dehghan, M., Fully spectral collocation method for nonlinear parabolic partial integro-differential equations, Applied Numerical Mathematics, 123, 99-120, 2018.
[21] Gatica, G.N., Munar, M. and Sequeira, F.A., A mixed virtual element method for the Navier-Stokes equations, Mathematical Models and Methods in Applied Sciences, 28(14), 2719-2762, 2018.
[22] Gatica, G.N., Munar, M. and Sequeira, F.A., A mixed virtual element method for a nonlinear Brinkman model of porous media flow, Calcolo, 55, 1-36, 2018.
[23] Goswami, D., Pani, A.K. and Yadav, S., Optimal error estimates of two mixed finite element methods for parabolic integro-differential equations with nonsmooth initial data, Journal of Scientific Computing, 56, 131-164, 2013.
[24] Guo, H. and Rui, H., Least-squares Galerkin procedures for parabolic integro-differential equations, Applied Mathematics and Computation, 150(3), 749-762, 2004.
[25] Guo, R., On the maximum angle conditions for polyhedra with virtual element methods, arXiv preprint arXiv:2212.07241, 2022.
[26] Jain, R., Pani, A.K. and Yadav, S., HDG method for linear parabolic integro-differential equations, Applied Mathematics and Computation, 450, 127-987, 2023.
[27] Jiang, Z., $L^\infty(L^2)$ and $L^\infty(L^\infty)$ error estimates for mixed methods for integro-differential equations of parabolic type, ESAIM: Mathematical Modelling and Numerical Analysis, 33(3), 531-546, 1999.
[28] Liu, Y., Fang, Z., Li, H., He, S. and Gao, W., A new expanded mixed method for parabolic integro-differential equations, Applied Mathematics and Computation, 259, 600-613, 2015.
[29] Medlock, J. and Kot, M., Spreading disease: integro-differential equations old and new, Mathematical Biosciences, 184(2), 201-222, 2003.
[30] Miller, R.K., An integrodifferential equation for rigid heat conductors with memory, Journal of Mathematical Analysis and Applications, 66(2), 313-332, 1978.
[31] Pani, A.K. and Peterson, T.E., Finite element methods with numerical quadrature for parabolic integrodifferential equations, SIAM Journal on Numerical Analysis, 33(3), 1084-1105, 1996.
[32] Pani, A.K. and Yadav, S., An hp-local discontinuous Galerkin method for parabolic integro-differential equations, Journal of Scientific Computing, 46, 71-99, 2011.
[33] Polyanin, P. and Manzhirov, A.V., Handbook of integral equations, Chapman and Hall/CRC. 2008
[34] Radid, A. and Rhofir, K., Partitioning differential transformation for solving integro-differential equations problem and application to electrical circuits, Mathematical Modelling of Engineering Problems, 6(2), 235-240 2019.
[35] Sinha, R.K., Ewing, R.E. and Lazarov, R.D., Mixed finite element approximations of parabolic integro-differential equations with nonsmooth initial data, SIAM Journal On Numerical Analysis, 47(5), 3269-3292, 2009.
[36] Sukumar, N. and Tabarraei, A., Conforming polygonal finite elements. International Journal for Numerical Methods in Engineering, 61(12), 2045-2066, 2004.
[37] Tang, X., Liu, Z., Zhang, B. and Feng, M., On the locking-free three-field virtual element methods for Biots consolidation model in poroelasticity, ESAIM: Mathematical Modelling and Numerical Analysis, 55, 909-939, 2021.
[38] Tushar, J., Kumar, A. and Kumar, S., Virtual element methods for general linear elliptic interface problems on polygonal meshes with small edges, Computers & Mathematics with Applications, 122, 61-75, 2022.
[39] Vacca, G. and Beirão da Veiga, L., Virtual element methods for parabolic problems on polygonal meshes. Numerical Methods for Partial Differential Equations, 31(6), 2110-2134, 2015.
[40] Yadav, S., Suthar, M. and Kumar, S., A Conforming Virtual Element Method for Parabolic Integro-Differential Equations. Computational Methods in Applied Mathematics, 2023.

Department of Mathematics, Birla Institute of Technology and Science, Pilani, India
E-mail: p20190039@pilani.bits-pilani.ac.in

Department of Mathematics, Birla Institute of Technology and Science, Pilani, India
E-mail: sangita.yadav@pilani.bits-pilani.ac.in